T.C.
ANTALYA BILIM UNIVERSITY
INSTITUTE OF POSTGRADUATE EDUCATION
ELECTRICAL AND COMPUTER ENGINEERING
THESIS PROGRAM

COMPUTER AIDED LUNG CANCER DIAGNOSES WITH DEEP LEARNING ALGORITHMS

DISSERTATION

Prepared By

Syed Nabeel AHMED

ANTALYA - 2020

T.C.
ANTALYA BILIM UNIVERSITY
INSTITUTE OF POSTGRADUATE EDUCATION
ELECTRICAL AND COMPUTER ENGINEERING
THESIS PROGRAM

COMPUTER AIDED LUNG CANCER DIAGNOSES WITH DEEP LEARNING ALGORITHMS

DISSERTATION

By

Syed Nabeel AHMED

Dissertation Advisor
Asst. Prof. Dr. Shahram TAHERI

ANTALYA - 2020

APPROVAL/NOTIFICATION FORM
ANTALYA BİLİM UNIVERSİTY
INSTITUTE OF POST-GRADUATE EDUCATION

SYED NABEEL AHMED, a M.Sc. student of Antalya Bilim University, Institute of Post Graduate Education, Electrical and Computer Engineering owning student ID 181212010, successfully defended the thesis/dissertation entitled "**Computer Aided Lung Cancer Diagnoses with Machine Learning**", which he prepared after fulfilling the requirements specified in the associated legislations, before the jury whose signatures are below.

Academic Tittle, Name-Surname, Signature

Thesis Advisor (Chairman): Asst**.** Prof. Dr. Shahram Taheri **..**……..

Jury Member: Asst. Prof. Jehad HAMAMREH, …….

Jury Member: Asso. Prof. ÜMİT DENİZ ULUŞAR …….……

Date of Submission: 03/11/2020
Date of Defense: 19/11/2020

Director of the Institute : Prof. Dr. İbrahim Sani MERT ……

DEDICATION AND ACKNOWLEDGMENT

I dedicate this thesis to my parents, friends, and teachers who always supported me to this day of my life.

I am very grateful to my advisor Asst. Prof. Dr. Shahram Taheri who guided and encouraged me throughout the thesis, who opened the doors for me in this field of research.

I would also like to thank the jury members Asso. Prof. Ümit Deniz ULUŞAR and Asst. Prof. Dr. Jehad Mahmoud HAMAMREH

ACADEMIC DECLARATION

I hereby declare that this master's thesis titled "Computer Aided Lung Cancer Diagnoses With Deep Learning Algorithms" has been written by myself under the academic rules and ethical conduct of the Antalya Bilim University.

I also declare that the work attached to this declaration complies with the university requirements and is my work.

I also declare that all materials used in this thesis consist of the mentioned resources in the reference list. I verify all these with my honor.

03/11/ 2020

Syed Nabeel Ahmed

ÖZET

DERIN ÖĞRENME ALGORITMALARI ILE BILGISAYAR DESTEKLI AKCIĞER KANSERI TEŞHISI

Kanser; şu anda dünyanın en ölümcül hastalıklardan biridir ve erken evrelerde teşhis edilmediği takdirde hastaları ölüme sürükler. Yani kanserin teşhisi, değerli insan hayatları için bir ölüm kalım meselesidir. Önde gelen kanser türlerinden biri de akciğer kanseridir ve bu kanserin teşhisi, yalnızca, her bir doktorun aldığı eğitim ile edindiği tecrübeye bağlıdır. Hastaların hayatı ile doğrudan bağlantılı olan bu sınırlamanın üstesinden gelmek için; yüzlerce doktorun ve radyoloğun deneyimine sahip olacak, bilgisayarlaştırılmış bir akciğer teşhis algoritması yapmak gerekmektedir. Bu sayede daha iyi teşhis olasılığı artabilir ve sayısız hayat kurtarılabilir. Bu proje, bu konu üzerine daha önce yapılmış çalışmalardan geçer; şimdiye kadar yapılan çalışmaların doğruluk oranını geçmek ve mümkün olan en iyi sonuca ulaşmak için, çok sayıda yoğun araştırmayı ve sıkı hazırlanmış yapay zekaları test eder. Bu projede kullanılan veri kümesi araştırma amacı ile internetten halka açılmış olan LIDC (Akciğer Görüntüsü Veritabanı Konsorsiyumu) veri kümesidir.

ABSTRACT

COMPUTER AIDED LUNG CANCER DIAGNOSES WITH DEEP LEARNING ALGORITHMS

Cancer is one of most deadliest diseases in the world right now, and if not diagnosed in early stages, it leads to death of the patients, which means diagnosis of cancer means life or death for precious human lives, one of the leading cancer types is lung cancer, and diagnosis of lung cancer solely depends on the education and experience of individual doctors and radiologists in current world. In order to overcome this limitation as it is directly related to the life of patient, a computerized lung cancer diagnosis algorithm is to be made which will have experience of hundreds of doctors and radiologists to refer from hence increasing the probability of better diagnosis and save countless lives. This project goes through past works done on this topic, tests numerous deep learning and hard crafted machine learning algorithms in order beat past highest accuracies and achieve the highest accuracy possible, the dataset used in this project is the LIDC dataset which is publically available for research purposes on the internet.

CONTENTS

LIST OF FIGURES

LIST OF TABLES

ABBREVIATIONS

BPPC	Binary Pattern of Phase Congruency
CAD	Computer Aided Diagnosis
CNN	Convolutional Neural Network
CT	Computed Tomography
FDA	Food and Drug Administration
FNIH	Foundation for the National Institutes of Health
GDP	Gradient Directional Pattern
GLTP	Gradient-Based Ternary Texture Pattern
HOG	Histogram of Oriented Gradients
IWBC	Improved Weber Binary Code
JPEG	Joint Photographic Experts Group
LAP	Local Arc Pattern
LBP	Local Binary Patterns
LDCCT	Low Portion Chest Figured Tomographic Filtering
LdiP	Local Directional Pattern
LdiPV	Local Direction Pattern Variance
LDN	Local Directional Number Pattern
LGBPHS	Local Gabor Binary Pattern Histogram Sequence
LGIP	Local Gradient Increasing Patter
LGP	Local Gradient Pattern
LIDC	Lung Image Database Consortium
LMP	Local Monotonic Pattern
MBC	Monogenic Binary Coding
MNIST	Modified National Institute of Standards and Technology
MRELBP	Median Robust Extended Local Binary Pattern
MTP	Median Ternary Pattern
NCI	National Cancer Institute
OTV	Large Pattern Vector
PET	Positron outflow tomography
RGB	Red Green Blue
SMPE	Stage Miniaturized Scale Extraction
TV	Pattern Vectors
VRC	Visual Recognition Challenge
WHO	World Health Organization
WLD	Weber Local Descriptor
XML	Extensible Markup Language

CHAPTER I

1.1 Introduction

Cancer is one of the world's most genuine medical conditions. Cancer leads to the death of

Million people worldwide by 2012. The death rate because of lung cancer amongst other cancers is the largest, affecting approximately 1.3 million people every year [1]. The death rate from lung cancer has just gone up to the most important of all cancers on earth, as indicated in the World Health Organization (WHO) study. More than 25% of all cancer- related passages are liable and more than combined breast, colon and prostate cancers are destroyed.[2]

One of the most well-known and most common forms of cancer amongst all cancers is the lung cancer. In the initial periods of lung cancer there are generally no signs or incidents but many people with the disease have other symptoms in the long term: [3]

- Persistent cough
- Blood while coughing
- Breathing difficulties
- Unexplained fatigue and weight loss
- It hurts while breathing or coughing

Lung cancer is mostly categorized in two types, these classifications are done based on which type of cells the cancer starts in. Following are the categories.

1) Big-cell: the type of lung cancer that is most common. where 80 percent of This group includes confirmed cases, these Either squamous, adenocarcinoma, or larger cell carcinoma may be present

2) Small-cell: small cell cancer is more of a scattered and less common type of lung cancer which is more deadly and spreads very quickly.

1.2 Motivation

When it comes to the diagnoses of the lung cancer it totally depends on education and the experience level of the radiologist and the concerned doctor, depending on how good his knowledge is in the field and the experience hence there have been several cases all around the world where patients were wrongly diagnosed or late diagnosed, leading to critical conditions of the patients, as we all are aware that in medical there is no room for error and even slight mistakes can lead to crucial if not disastrous results where patients can lose their life.

In order to overcome such problems, a computer diagnosis algorithm is being proposed using CNN (convolutional neural network) a machine learning technique, if this proposed software is successful, it will be equal to hundreds or thousands of doctor's experience hence reducing the ill diagnosis chances improving the medical diagnosis area which can be extremely beneficial for patients who might get diagnosed in really early stages and get treatment before cancer gets out of hand.

1.3 Contribution

We investigated 23+ different architectures in both deep learning and hand crafted domain and tried to find the optimal setting for each of the method. These architectures have been invented by other authors for texture extraction or face recognition, facial expression recognition but never used in this domain, we believe they can be beneficial in this domain. Since previously achieved maximum accuracy was 97%, we managed to obtain 98.18% accuracy. If implemented in real healthcare applications the 1.18% increased accuracy means more patients can be diagnosed correctly, as this topic is directly related to cancer diagnosis, these better diagnosis will save more lives.

CHAPTER II

2.1 Related Work

"Medical and biological engineering protocol 2005 IEEE Annual Conf 27th. 27th. Sep 1-4 "China [4] proposed a noninvasive locational technique for lung malignancy joined with a form of SAW gas sensor virtual and imagery recognition strategy. Patients inhale experiences electrical nose with strong stage miniaturized scale extraction (SMPE) and hair like section for pre- concentration and division of unpredictable natural mixes (VOCs) individually. “Noha Lee” [5] gives understanding into viability of lung malignancy screening and evaluates the capability of compute raided plan improvements. CAD design frameworks for lung tissue segregation, knob separation, and knob portrayal. Designing of CAD Technology may very much assist radiologists with adjusting the advantage cost analytics of CT affectability and explicitness in lung malignancy screening. “David S paik” [6] created CAD calculation to identify lung knob and polyp identification utilizing CAD ordinary surface cover technique in helical Computed Tomography (CT) pictures. Histological subsets and various components will substantially increase homogeneity and improve predictive consistencies. In particular in those patients suffering from early infection due to poor prognostic factors, the capacity for long-haul endurance is decreased. The increasingly accurate predictions that explain the research needed for critical and adjuvant care.

“Jyh-Shyan” [7] built up a neural- computerized computer aided finding framework (CAD) framework dependent on a defined 2-level convolutional neural system (CNN) Architecture and on an exceptional ability to be multiplied yield encoding method. The created engineering was prepared, tried and assessed extraordinarily on the issue of finding of lung malignant growth knob found on digitized chest radio-charts. The framework performs programmed speculate confinement highlight extraction and analysis of a specific example class-focused on a serious extent of “genuine positive part” recognition and “low positive portion” discovery. “M. Freedman [8] evaluated the recognition of signs reliable to lung malignancy on chest scans and bosom disease on the

mammogram. There are frameworks for different sicknesses and different sorts of pictures a work in progress; be that as it may,this procedure relies upon the accessibility of a precise database . The exhibition of a CT CAD Siemen's Lung Care framework against a doctor or radiologist's produced database of CT imaged knobs. Computer aided de- sign and individual radiologists taking an interest in the assessment performed comparatively. "R. MacRedmond," [9] introduced the commonness of good lung malignancy distinguished by using the LDCCT architecture at pattern screening was as low as 0.23%, but high pace of noteworthy coincidental pathology came forward. Low Portion Chest Figured Tomographic Filtering (LDCCT) is able to distinguish beginning time asymptomatic disease of lung in a highly hazardous urban population. 400 forty patients experienced medical procedure for essential lung malignancy, and there 45 typical cases of this were chosen. Total 8 radiologists took an interest in eyewitness tests. "Basavanna" [10] gave rules to clinically applicable FPR and TPR measures [11] just as extraordinary ROC techniques for malignancy screening, [12-13] and furthermore noticed that since the hidden predominance of disease in normal hazard populaces is low, the FPR ought to be exceptionally little for adequate malignant growth screening of asymptomatic individuals. "Bhagyasri G. Patil" [12], the creators depicted a hypothetical investigation on the most proficient method to join classifiers with an ideal choice standard and ideal ROC bend. To give clinically important definitions to affectability and explicitness [14-15].

"Aparna Kanakatte" [16] depicts Lung carcinoma is among one of the most deadliest of diseases all around the world. Positron outflow tomography (PET) information has more prominent affectability and explicitness the organizing of malignant growth in lung than registered CT or MRI. By utilizing adjacent neighbor and SVM classifiers. Wavelet highlights along with SVM classifier gave a predictable accuracy of 97 %. "Yongbum Lee" [17] proposed novel layout coordinating strategy dependent on hereditary algorithm(GA) format coordinating (GATM) for distinguishing knobs existence in lung zone, CAD frameworks to identify lung knob in the helical X-beam pneumonic processed

tomography pictures. GA was utilized to decide the objective situation in watched picture productively & to choose a sufficient format picture from database. By utilizing this strategy discovery of knob rate is about 72%.

Samuel H Hawkins [18] introduced on concentrating the instances of adenocarcinoma non-small-cell lung malignant growth tumor subtype, from a bigger informational collection. Relationship of classifiers for the future choice methodologies. Classifiers are utilized to work to foresee endurance time.

"Anam Tariq" [19] explored the impact of CAD plot on radiologist execution in recognition of lung malignant growths on chest scans. "Detection of Lung cancer in CT Images using Mean Shift Algorithm" [20] revealed a CAD framework for knob location utilizing a distinction picture procedure. They looked at a few guideline based plans for distinguishing knobs. A gigantic preparing ANN (MTANN) [21] decreased the bogus positives. "Dansheng Song" [13] wrote about a CAD plan to assist radiologists with improving the discovery of pneumonic knobs in chest scans by concentrating on bogus positive decrease. They can lessen the quantity of bogus positive to as low as 44.3% with little increment in quantity of genuine positive by 2.3%. "Kesav Kancherla" [22], got an exactness of 81% utilizing 71 highlights identified with shape, force and shading in our past work. By including the core sectioned highlights we have improved precision to 87 %. Core division is done by utilizing seeded area developing division technique. Our outcomes exhibit the capability of core divided highlights for distinguishing lung malignant growth in beginning time. "R. Sah.," [23] Multiyear endurance in stage 1, carcinoma was not impacted by histological kind, and there was factually noteworthy contrast in endurance between adenocarcinoma and squamous cell carcinoma in stage 2 sickness, with beginning time lung malignancy announced models specific to patient for recognizing lung knobs to be used in screening and later on in follow-up observation. In the most recent decades, an enormous group of examination has been accounted for in field of lung knob location and characterization [17]. "S. Sone" [24] most lung malignant growths are not confined when previously identified, however early location is required to increase guess. Since treatable early stage cases are difficult to envision with customary chest scans, another

demonstrative methods has to be found. We surveyed whether population based, mass screening of patients with a winding figured tomography scanner could contribute considerably to the discovery of littler tumors, and diminishing mortality. “Cancer screening” [25] depicted a mechanized technique to recognize kindhearted and dangerous single knobs. 55 chest scans were separated utilizing ANN & LDA for highlight blend and order. Correlations with the manual evaluating demonstrated that LDA had AUC estimation of 88.6 %, while manual ID brought about AUC estimation of 85.4%. “Survival in early- stage lung cancer” [26] Decreasing morphologic contrasts by setting patients in bunches dependent on TNM subsets & refinement in classification by coordinating TNM “Survival from early lung cancer: Implications for screening” [27] 70 % of the stage 1 patients in every program who were dealt with carefully endure over 5 years, yet there were just two 5- year survivors among the individuals who didn’t have medical procedure. We infer that people with lung malignant growths recognized in stage 1 by chest x-beam film & rewarded carefully have decent possibility of staying liberated from ailment for a long time. Those stage 1 lung malignant growths which were not regarded progress & leaded to death within 5 years. In this way, every exertion ought to be made in order to recognize and treat the lung malignancy from the get-go in high-chance populaces. A focal worry in knob discovery is high pace of bogus positive, when affectability is expanded to distinguish inconspicuous knobs. A knob is regarded a bogus positive outcome in the event that it prompted a totally negative workup or over a year of catch up with no malignant growth determination. Diminishing bogus positive rates while keeping up high affectability is as yet a troublesome issue. Information mining methods incorporate LDA [21], rule based approaches (a lot of “assuming at that point” proclamations), blends of the two [28], fake neural systems (ANN), and discriminators based greatest edge, for example, is SVM. Unique systems for looking are presented. Coordinating for location [27], unaided grouping methods [29], and a neighborhood thickness greatest calculation [30]. Techniques in order to improve segregation of knobs from tissues of lung incorporate deduction of vessels district by district developing.

Table 1– Summary of Past work results

WORK	Classifier	Accuracy
[10]	Classification	72%
[25]	SVM	80.36%
[19]	KNN, DT	85%
[28]	SVM	85%
[24]	Classification	85.25%
[23]	Mathematical Morphology	86%
[29]	Back Propagation Network	86.30%
[31]	Random forest	87%
[20]	Bayesian	88.62%
[26]	Neuro-fuzzy	95%
[30]	ANN	95%
[21]	KNN, SVM	97%
[8]	KNN, SVM	97%

Table 2 – Another table for work done in this domain [68]

Author	Year	Accuracy (%)	Sensitivity (%)	Classifier	Nodule Type	Selected Features
Akram et al	2015	96.6	96.9	SVM	All types	2D and 3D geometric and intensity statistical features
El Regaily et al	2017	70.5	77.7	The simple rule classifier	All types	Geometric and intensity statistical features
Gonçalves et al	2018	68.4	55	SVM	Solid nodules	Intensity-, texture-, and shape-based features
Gong et al	2016	91.5	90.2	FLDA	Not GGO	11 selected image features
Hancock et al	2017	88	84.6	Nonlinear	All types	Nonlinear classifier, diameter, and volume features included
Shaukat et al	2017	97.1	98.1	SVM-Gaussian	All types	Intensity, shape (2D and 3D), and texture features
Ta¸scı et al	2015	92.9	-	GLMR	Juxtapleural	Seven shape- and texture-based features
Wang et al	2018	95.9	95.6	SS-ELM	All types	Haralick features and morphological features
Zhao et al	2017	91.2	-	softmax	All types	Global and local features

CHAPTER III

3.1. Method

Machine learning is a branch of artificial intelligence, a science that explores machines by learning from existing dataset to get new information, new skills and new abilities and to distinguish existing information. Machine learning is mostly used in computer vision, data mining, strategy games, biometrics, robotics, DNA sequence sequencing, speech and handwriting recognition, detection of credit card fraud, medical diagnostics, securities market analysis, search engines & natural language processing. [31]

Machine learning mainly is classified into following:

1. Unsupervised learning: Info information has no labels, yet calculations to gather the characteristic connections of information, for example, grouping and affiliation rule learning. Regular calculations incorporate autonomous segment examination, Apriority and K-Means calculations.

2. Supervised learning: Input information is labeled. Managed learning sets up a learning procedure, contrasts the anticipated outcomes and the genuine aftereffects of the "preparation information" (i.e., input information), and ceaselessly modifies the prescient model until the anticipated consequences of the model arrive at a normal exactness, for example, order and relapse issues. . Normal calculations incorporate choice trees, Bayesian order, least squares relapse, strategic relapse, bolster vector machines, neural systems, etc.

3. Semi-supervised learning: input information part labels, is augmentation of regulated learning, regularly utilized for characterization & relapse. Normal calculations incorporate diagram hypothesis deduction calculations, Laplacian bolster vector machines, etc.

4. Reinforcement learning: Information as criticism to the model, underscoring the proper behavior dependent on the earth to expand the normal advantages. The distinction between regulated learning is that it doesn't require the right information/yield matches and doesn't require exact revision of imperfect conduct. Support learning is progressively centered on web based arranging and requires a harmony between investigation (in the obscure) and consistence (existing information).

3.2. Convolutional Neural Networks (CNN)

An exemplary use instance of CNNs is to perform picture characterization, for example taking a glance at a picture of a house pet and concluding whether it's a feline or a canine. It is apparently straightforward undertaking. The used images can be big, Pictures utilized for Computer Vision issues these days are regularly 224x224 or bigger. Envision constructing a neural system to process a 224x224 shading pictures: with the 3 shading channels (RGB) in picture, this becomes 224 x 224 x 3 = 150,528 info highlights! A run of the mill shrouded layer in such a system may have 1024 hubs, so we would need to prepare 150,528 x 1024 = 150+ million loads for the principal layer alone. Our system would be gigantic & very difficult to prepare. [32]

And it is unlikely we need that numerous loads, either. The pleasant thing about pictures is that we realize pixels are generally helpful with regards to their neighbors. Articles in pictures are comprised of little, restricted highlights, similar to the round center of an eye or the square corner of a paper. Doesn't it appear to be inefficient for each hub in the principal concealed layer to take a gander at each pixel?

Positions of the needed object can change on the off chance that you prepared a system to recognize hounds, you'd need it to have the option to distinguish a canine where it shows up in the picture. Envision preparing a system that functions admirably on a specific pooch picture, however then taking care of it a somewhat moved adaptation of a similar picture. The canine would not actuate similar neurons, so the system would respond totally in an unexpected way.

They're essentially simply neural systems that utilization Convolutional layers, (Conv layers) which depend on scientific activity of convolution. Convolutional layers are comprised of lots of channels, which you may consider as just 2 dimensional lattices of numbers. Here is an example of a 3x3 filter:

-1	0	1
-2	0	2
-1	0	1

We can utilize an info picture and a channel to create output image with convolving the channel on input image. This comprises of

- Overlaying the channel on the picture at some area.
- Performing component insightful augmentation between the qualities in the channel and their comparing esteems in the picture.
- Summarizing all the component astute items. This entirety is the yield an incentive for the goal pixel in the yield picture.
- Rehashing for all areas.

That 4-advance portrayal was somewhat conceptual, so we should look at an example. Consider this small 4x4 grayscale picture and this 3x3 channel:

0	20	23	66
0	96	12	65
24	45	54	32
0	331	74	72

-1	0	1
-2	0	2
-1	0	1

A 4x4 picture (on left-side) and a 3x3 channel (on right-side)

The numbers in the picture speak to pixel powers, where 0 = black and 255 = white. We will convolve the info picture & the channel to create a 2x2 output image, let’s start with overlaying the filter on top-left corner of image:

0	20	23	66
0	96	12	65
24	45	54	32
0	331	74	72

Next, we perform multiplication to each overlapping elements of both the source image and the filter. These are the outcomes, starting from top-left corner and going towards right, at that point down:

Table 3 - Outcomes of CNN explanation example

Source	Filter	Outcome
0	-1	0
20	0	0
23	1	23
0	-2	0
96	0	0
12	2	24
24	-1	-24
45	0	0
54	1	54

Now we just simply add up all results:

23 + 24 – 24 + 54 = 77

Now, we put our outcome in goal pixel of the output image. Since the filter is overlaid in upper left corner of our source image, & our goal pixel is upper left pixel of output image:

0	20	23	66
0	96	12	65
24	45	54	32
0	331	74	72

77	?
?	?

This is an example of the vertical Sobel filter.

Since we learned how picture convolution functions and why it's helpful, how about we perceive how it is really utilized in CNNs. As referenced previously, CNNs incorporate convolutional layers that utilization a lot of channels to transform input pictures into yield pictures. A convolutional layer's essential boundary is the quantity of channels it has.

For our MNIST CNN, we will utilize a little convolutional layer with a total of 8 filters as the underlying layer in our system. This implies it'll transform the 28x28 source image into 26 x 26 x 8 output volume.

Every one of 8 channels in the convolutional layer creates a 26 x 26 output, so after stacked together, they make up a 26 x 26 x 8 volume. The entirety of this, happens in view of 3\times

× 3 (filter size) \ times × 8 (# of filters) = only 72 weights.

Now talking about pooling in CNN, Neighboring pixels in pictures will in general have similar qualities, so convolutional layers will ordinarily additionally create comparative qualities for neighboring pixels in yields. Thus, a significant part of the data contained in a convolutional layer's yield is excess. For instance, in the event that we utilize an edge-distinguishing channel and locate a solid edge at a specific area, odds are that we'll likewise discover generally solid edges at areas 1 pixel moved from the first one. Be that as it may, these are no different

edge! We're not discovering anything new.

Pooling layers take care of this issue. All they do is diminish the size of info it is given, pooling values together in the information. The pooling is generally done by a basic activity like normal, max or min. Here is a case of a Max Pooling layer with a pooling size of 2:

For max pooling, we navigate the information picture in 2x2 squares (since pool size = 2) And put the maximum incentive into the yield picture at the comparing pixel. That is it!

Pooling partitions the information's width and stature by pool size. For our MNIST CNN, we will place a Max Pooling layer, with pool size of 2, just after our underlying convolutional layer. The pooling layer will change 26 x 26 x 8 contribution to a 13 x 13 x 8 yield.

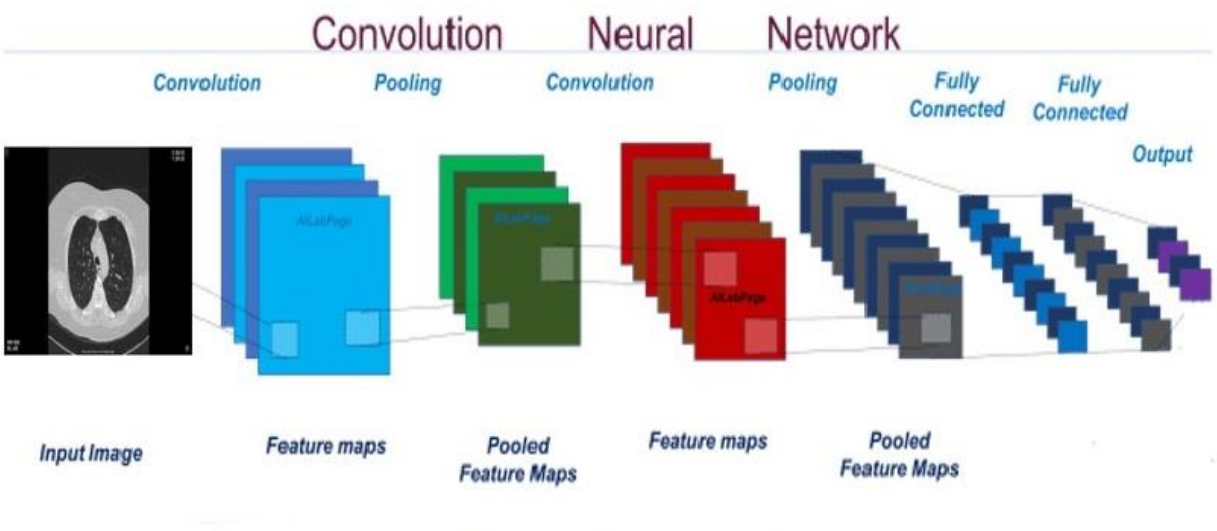

Figure 1 - CNN architecture

3.3. DataSet

The DataSet we used is LIDC dataset, which is publically available on internet for use of rese- arch purpose.

LIDC (The Lung Image Database Consortium) image collection comprises of symptomatic and lung malignancy screening thoracic computed tomography (CT) filters with amplified explained injuries. It is a web open global asset for preparing, improvement, and assessment of computer-assisted diagnostic (CAD) techniques for lung malignancy recognition and analysis. Started by National Cancer Institute (NCI), further progressed the Foundation for the National Institutes of Health (FNIH), and joined by Food and Drug Administration (FDA) through dynamic cooperation, this open private association exhibits the achievement of a consortium established on an accord based procedure. [33-34] 7 scholarly focuses and 8 clinical imaging organizations worked together to make this informational collection, it contains a total of 1018 cases. Each subject incorporates pictures from a clinical thoracic computed tomography check and a related XML document (Figure 1) that records the aftereffects of a two-stage picture comment process, done by 4 experienced thoracic radiologists. In the underlying blinded-read stage, every radiologist freely surveyed every CT examine and checked injuries having a place with one of three classifications ("nodule<3 mm", "nodule > or =3 mm," and "non-nodule"). In the ensuing unblinded-read stage, every radiologist autonomously assessed their own imprints alongside the anonymized signs of the three different radiologists in order to render a last sentiment. The objective of this procedure was to distinguish as totally as conceivable all lung knobs in every CT filter without requiring constrained accord.

The images of CT Scans are included in dataset are of different views and perspectives. Example Figure (2-8)

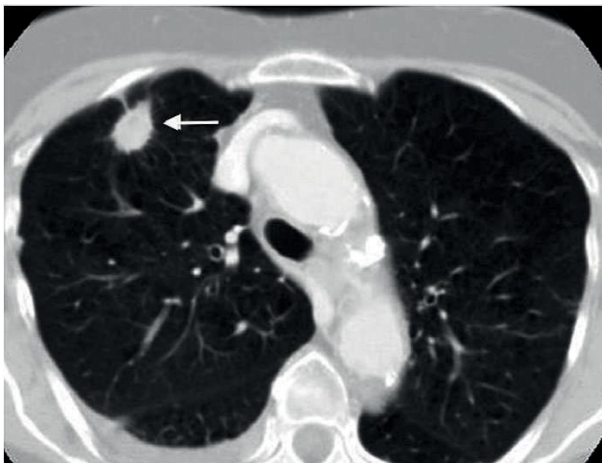

Figure 1 - Example of the CT scan images

Figure 2 - Example of the CT scan images

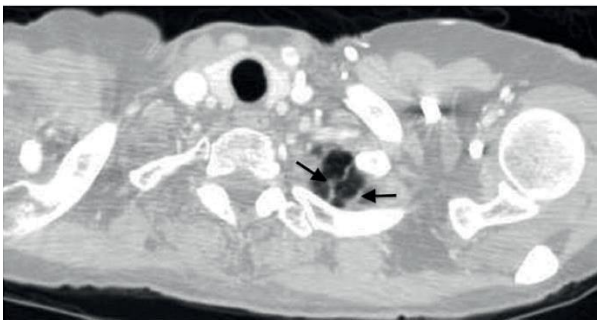

Figure 3 - Example of the CT scan images

Figure 4 - Example of the CT scan images

Figure 5 - Example of the CT scan images

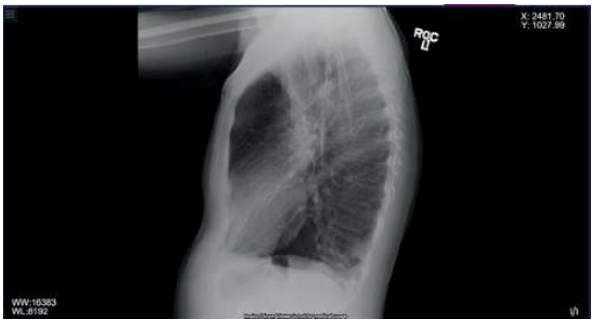

Figure 6 - Example of the CT scan images

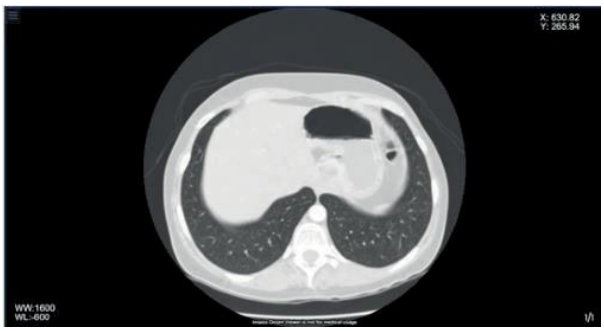

Figure 7 - Example of the CT scan images

Apart from XML files there are also various EXCEL files available containing further details of the patients, which type of nodules are there. Example Figure-9

TCIA Patent ID	Total Number of Nodules*	Number of Nodules >=3mm**	Number of Nodules <3mm***
LIDC-IDRI-0001	4	1	3
LIDC-IDRI-0002	12	1	11
LIDC-IDRI-0003	4	4	0
LIDC-IDRI-0004	4	1	3
LIDC-IDRI-0005	9	3	6
LIDC-IDRI-0006	14	4	10
LIDC-IDRI-0007	2	2	0
LIDC-IDRI-0008	4	2	2
LIDC-IDRI-0009	11	2	9
LIDC-IDRI-0010	6	3	3
LIDC-IDRI-0011	17	10	7
LIDC-IDRI-0012	16	12	4
LIDC-IDRI-0013	34	3	31
LIDC-IDRI-0014	3	1	2
LIDC-IDRI-0015	2	1	1
LIDC-IDRI-0016	14	6	8
LIDC-IDRI-0017	1	1	0
LIDC-IDRI-0018	6	4	2
LIDC-IDRI-0019	5	1	4
LIDC-IDRI-0020	4	2	2
LIDC-IDRI-0021	4	3	1
LIDC-IDRI-0022	4	1	3
LIDC-IDRI-0023	2	1	1
LIDC-IDRI-0024	5	4	1
LIDC-IDRI-0025	2	1	1
LIDC-IDRI-0026	27	2	25
LIDC-IDRI-0027	9	7	2
LIDC-IDRI-0028	1	0	1
LIDC-IDRI-0029	5	1	4
LIDC-IDRI-0030	22	2	20
LIDC-IDRI-0031	10	5	5
LIDC-IDRI-0032	3	0	3
LIDC-IDRI-0033	6	2	4
LIDC-IDRI-0034	8	1	7
LIDC-IDRI-0035	5	1	4
LIDC-IDRI-0036	6	2	4
LIDC-IDRI-0037	3	2	1
LIDC-IDRI-0038	1	1	0
LIDC-IDRI-0039	6	5	1
LIDC-IDRI-0040	8	4	4
LIDC-IDRI-0041	7	3	4

The total size of this data set is 124 Gigabytes and it consists of total 245,931 files including XML and scan Images, (figure 10)

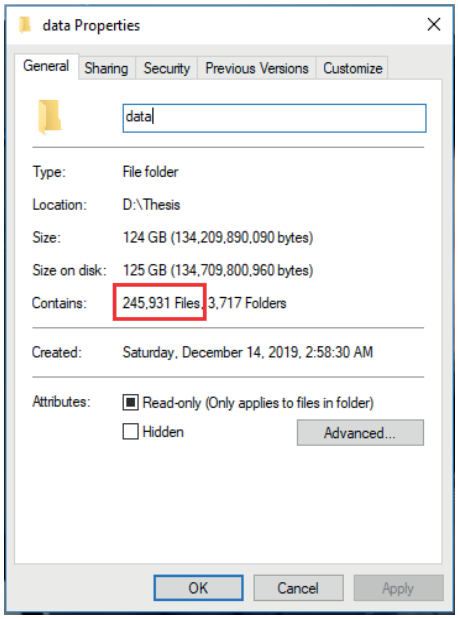

Figure 10 - Total size of the data set

With help of Nodule Counts by Patient (XLS) (figure 7) we categorized our dataset into 3 categories

1) Big Nodules (nodules >=3mm nodules)
2) Mix Nodules (containing both >=3mm and <3mm nodules)
3) No nodules (patients which does not have any nodules)

CHAPTER IV

4.1 Technique

Since our dataset is too large and we have no resources to train our system correctly across all data sets, Transfer Learning Technique is the technique we used here.

Transfer learning is an automated learning methodology where a model designed for a second similar task is re-assigned. Transfer learning is a development that makes rapid progress or better execution when the second task is demonstrated. [35]

In transfer learning, first we train a base system on a dataset and task, and subsequently recreate or pass the informed highlights to a subsequent objective system, which is prepared for an objective data set and mission. This technique will usually work if the highlights are common, indicating that both the foundation and the aim tasks are relevant and not unique to the basic task.

There are two common approaches in transfer learning, they are as follows:

1.1. Develop Model Approach

1.2. Pre-trained Model Approach

4.1.1 Develop Model Approach

1) Choose a source task: you can choose a specific display problem with a wealth of information in which information, information about the returns and additional ideas are linked to the mapping of the contribution to the information.

1) Design Source Model: next, create a convenient prototype for the first transaction. The model needs to be better than a credulous model to ensure that certain components are understood.

2) Reuse Model: The model installed on the source errand may then be used as the initial stage for a model for the second mystery undertaking. This can include the use of all or parts of the pattern, depending on the display technique used.

3) Tuning Model: the model may optionally be modified or refine on knowledge pairs accessible for the intrigue assignment.

4.1.2 Pre-trained Model Approach

1) Choose the model of the source: A pretrained model of the source is looked at over open models. Many research organizations dump large and testing datasets of models that could be reassembled to cover the pool of competitor models.

2) Model reuse: The pre-trained model could then be used as the beginning of a model for the second suspense assignment. The use of any or parts of the model could be dependent on the presentation method used.

3) Tuning Model: Instead, the input pair information obtained for the necessary task may have to be changed or improved.

We have experiments by testing various Pre-Trained models on a fraction of our dataset, because as we mentioned earlier we lack the resources of training and processing the entire dataset.

CHAPTER V

Experiment

We have experimented with two different machine learning approaches,

1) Deep Learning Architectures

   Pre trained architectures made to be used on different tasks, they select optimal setting according to the provided task, and these are included as transfer learning as they have already been trained and ready to perform on desired task.

2) Hand Crafted Descriptors

   Hand Crafted for specific tasks, have to be meddled with in order to perform another task, these are not pre trained and have to be trained before used on desired task which require big dataset and would not be optimal approach in case of limited or small dataset.

5.1 Deep Learning Architectures

The models we used in the experimental phase are;

i. Googlenet

ii. Resnet18

iii. Inceptionv3

iv. mobilenetv2

v. Resnet101

5.1.1. Googlenet

GoogLeNet is a pre-trained model trained in an ImageNet database subset which is used in the Visual Recognition Challenge (ILSVRC) ImageNet. The model has over one million images, 144 layers and is capable of classifying images into 1000 categories of objects. [35]

We split the sample dataset in 70% for training and 30% for testing, after running the test we got 92.04% accuracy, the result graph and confusion matrix are shown in figure 12-13.

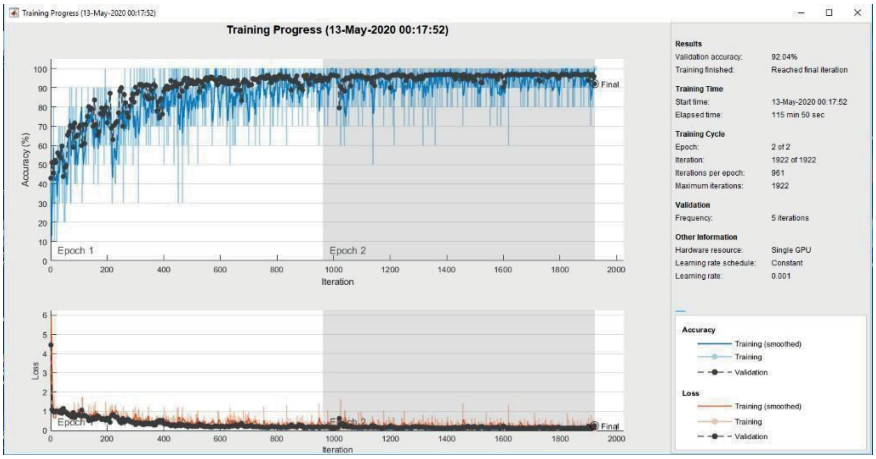

Figure 11 - Result graph for Googlenet model

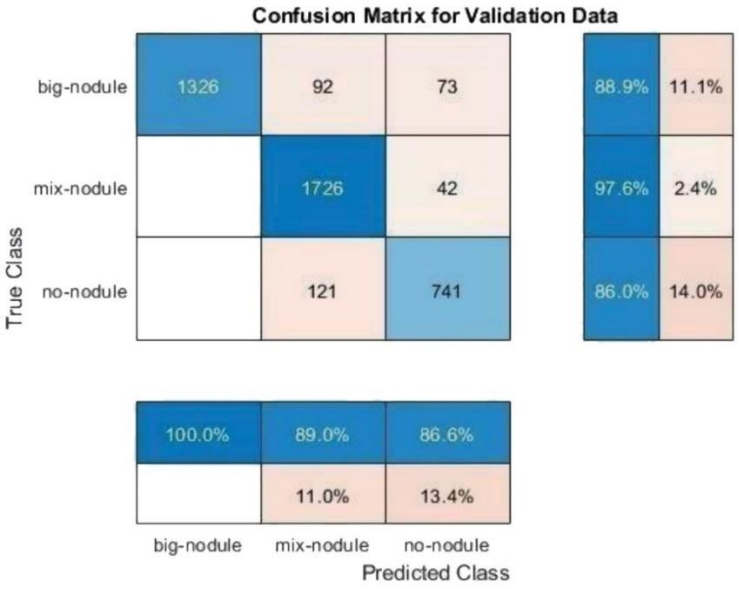

Figure 12 - Confusion matrix of Googlenet model

5.1.2 Resnet18

ResNet-18 is a convolutionary 18-layer neural network. You can store a pre-trained machine reproduction on over a million images from the Image-Net database. The pre-trained network will organize images to identify 1000 posts, for example consoles, mouse, pencils and many animals. The machine has therefore studied rich images of components for a wide range of data. The machine has a 224-by-224 image input size. [36]

After running the test we got 96.36% accuracy, the result graph and confusion matrix are shown in figure 14-15.

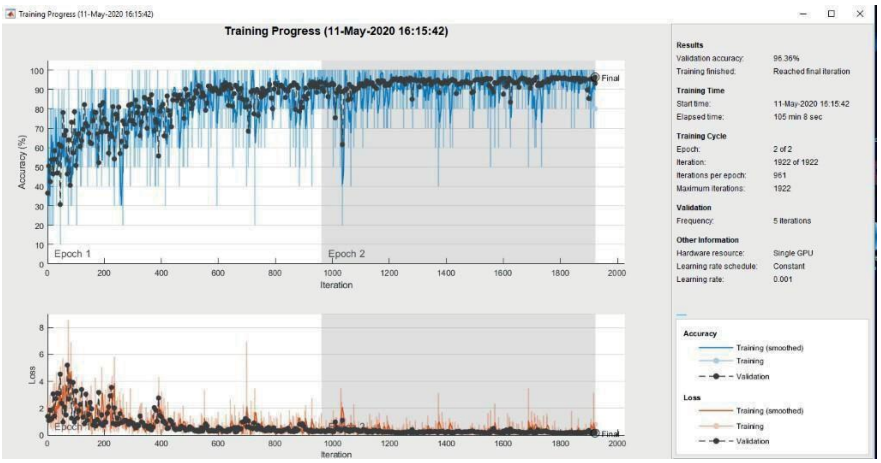

Figure 13 - Result graph for Resnet18

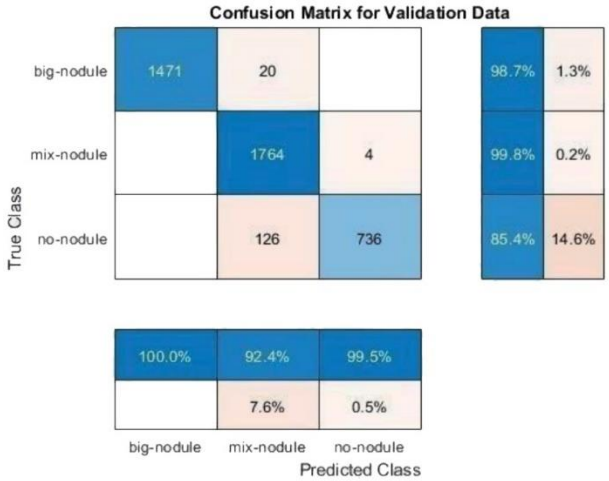

Figure 14 - Confusion matrix of Resnet18

5.1.3 Inceptionv3

Inceptionv3 is a convolutional neural network that is 48 layers deep. You can stack a pre-trained rendition of the system prepared on in excess of a million pictures from the ImageNet database. The pre-trained network can group pictures into 1000 item classes, for example, console, mouse, pencil, and numerous creatures. Accordingly, the system has learned rich component portrayals for a wide scope of pictures. The system has a picture input size of 299- by-299. [37]

After running the test we got 91.39% accuracy, the result graph and confusion matrix are shown in figure 16-17.

.

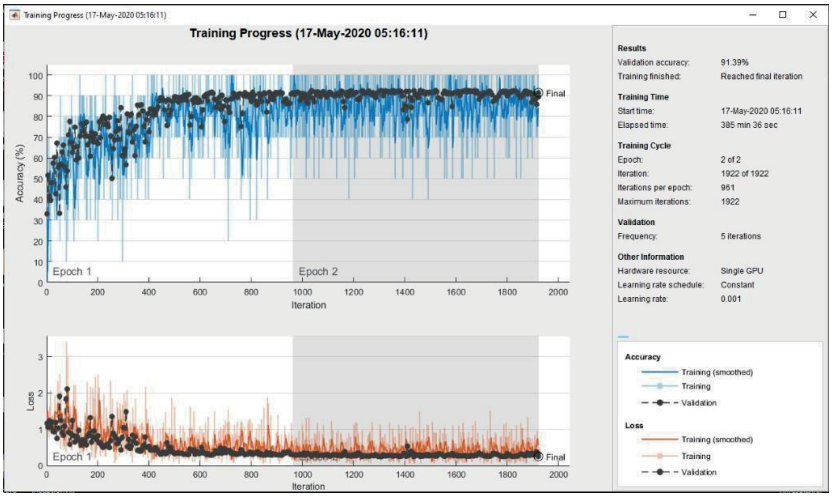

Figure 15 - Result graph for Inceptionv3

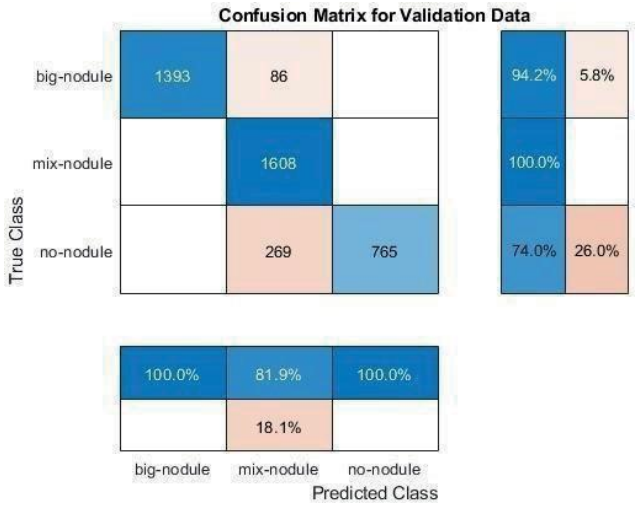

Figure 16 - Confusion matrix of Inceptionv3

5.1.4 Mobilenetv2

MobileNet-v2 is a convolutional neural network that is 53 layers profound. You can stack a pre- trained variant of the system prepared on in excess of a million pictures from the Image- Net database. The pre-trained network can arrange pictures into 1000 item classifications, for example, console, mouse, pencil, and numerous creatures. Therefore, the system has learned rich element portrayals for a wide scope of pictures. The system has a picture input size of 224- by-224. [38]

After running the test we got 96.97% accuracy, the result graph and confusion matrix are shown in figure 18-19.

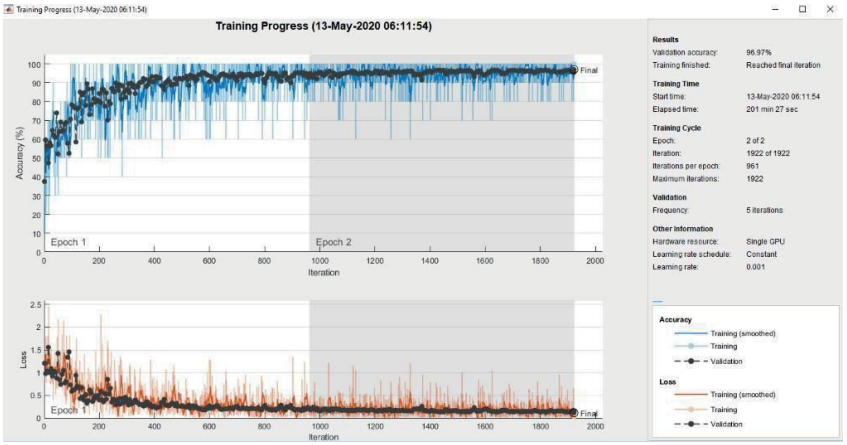

Figure 17 - Result graph for Mobilenetv2

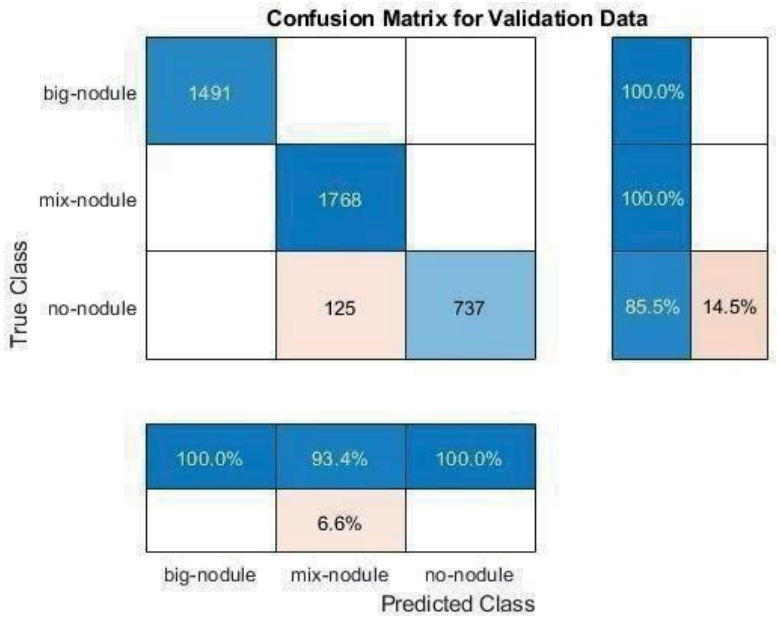

Figure 18 - Confusion matrix of Mobilenetv2

5.1.5 Resnet101

ResNet-101 is a convolutional neural network that is 101 layers profound. You can stack a pre- trained rendition of the system prepared on in excess of a million pictures from the ImageNet database. The pre-trained network can arrange pictures into 1000 article classifications, for example, console, mouse, pencil, and numerous creatures. Thus, the system has learned rich component portrayals for a wide scope of pictures. The system has a picture input size of 224- by-224. [39]

After running the test we got 96.97% accuracy, the result graph and confusion matrix are shown in figure 20-21.

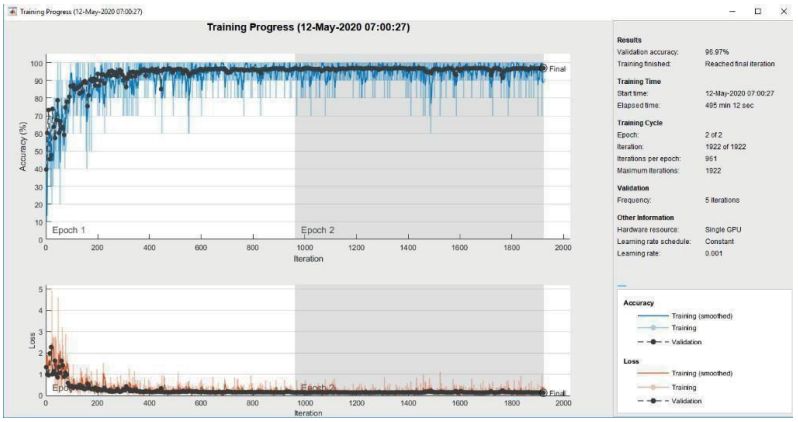

Figure 19 - Result graph for Resnet101

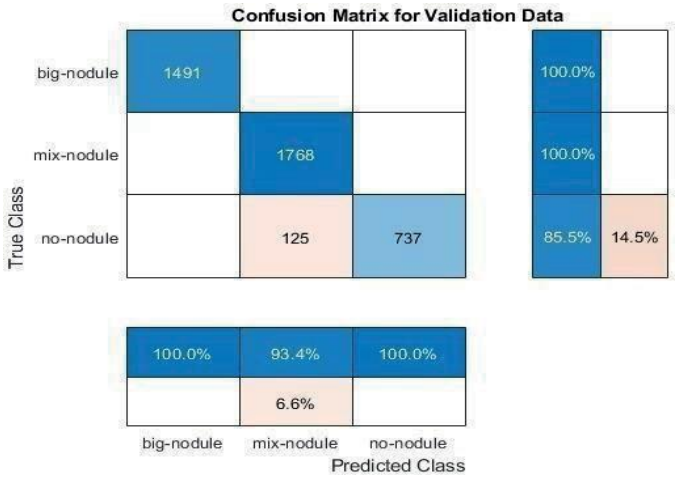

Figure 20 - Confusion matrix of Resnet101

Here is the summary table of all deep learning algorithm experiments:

Table 4 – summary of deep learning test results

MODEL	ACCURACY
Googlenet	92.04%
Resnet18	96.36%
Inceptionv3	91.39%
mobilenetv2	96.97%
Resnet101	96.97%

5.2. Hand Crafted Descriptors

The descriptors we used in the experimental phase are;

1) BPPC
2) GDP
3) GLTP
4) IWBC
5) LAP
6) LBP
7) LDiP
8) LDiPV
9) LDN
10) LGBPHS
11) LGP
12) LGiP
13) LMP
14) MBC
15) MRELBP
16) MTP
17) WLD
18) HOG

5.2.1. Binary Pattern of Phase Congruency (BPPC)

Binary pattern of phase congruency is a novel hand-crafted feature which used by combining LBP on PC images, this tool was initially constructed for facial expression recognition, and here in this project we use it lung cancer detection on lung scan images [40]. After testing this algorithm on 10% of our entire dataset (the small section that we used to test the accuracy of algorithms) we got 93.57 % accuracy.

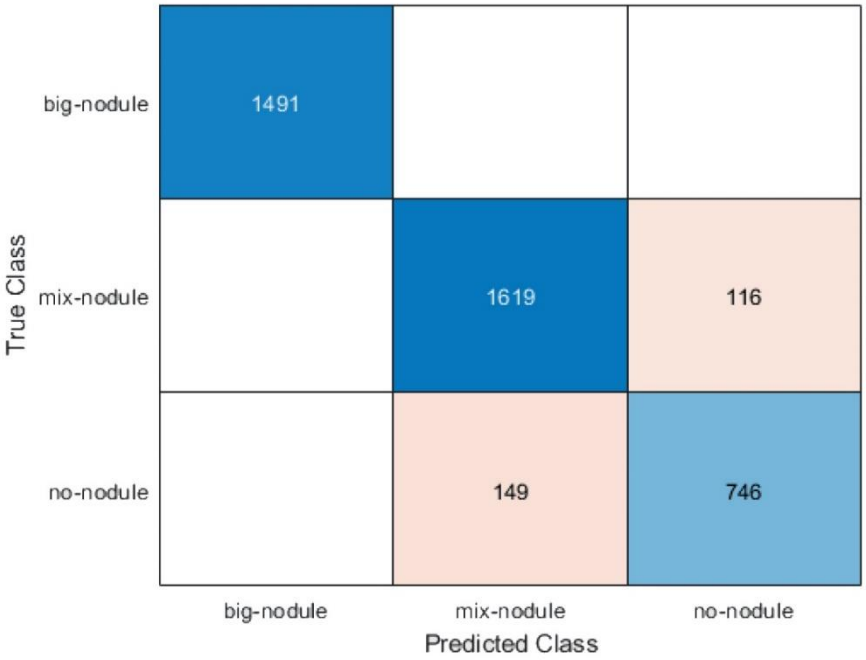

Figure 21 - Result of BPPC

5.2.2. Gradient Directional Pattern (GDP)

Gradient directional pattern is a novel hand crafted feature, this algorithm's operator encodes texture information of local regions by quantizing the gradient directional angles and form a binary pattern, due to this, GDP can retain more information as compared to other grey-level based methods and it can describe local images in a much more stable manner [41]. After testing this algorithm on 10% of our entire dataset (the small section that we used to test the accuracy of algorithms) we got 94.28 % accuracy.

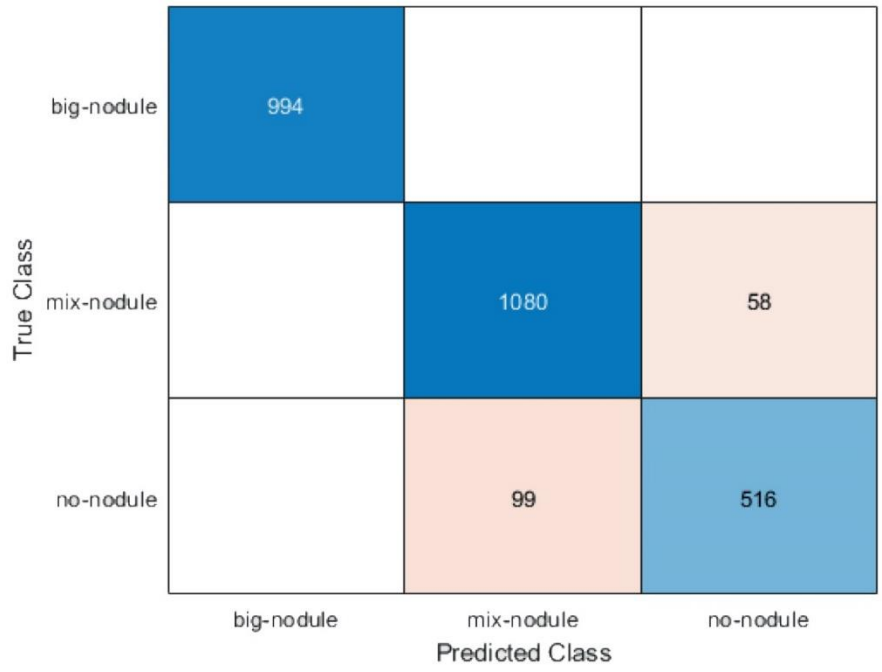

Figure 22 - Result of GDP

5.2.3. Gradient-Based Ternary Texture Pattern (GLTP)

Gradient-base ternary texture pattern is an algorithm where operators encodes the local texture of images by computing the gradient magnitude of neighboring nodes and quantizing into three discrimination levels, after that the occurrence and location data of the resulted micro patterns is used as face feature descriptor [42]. After testing this algorithm on 10% of our entire dataset (the small section that we used to test the accuracy of algorithms) we got 94.28 % accuracy.

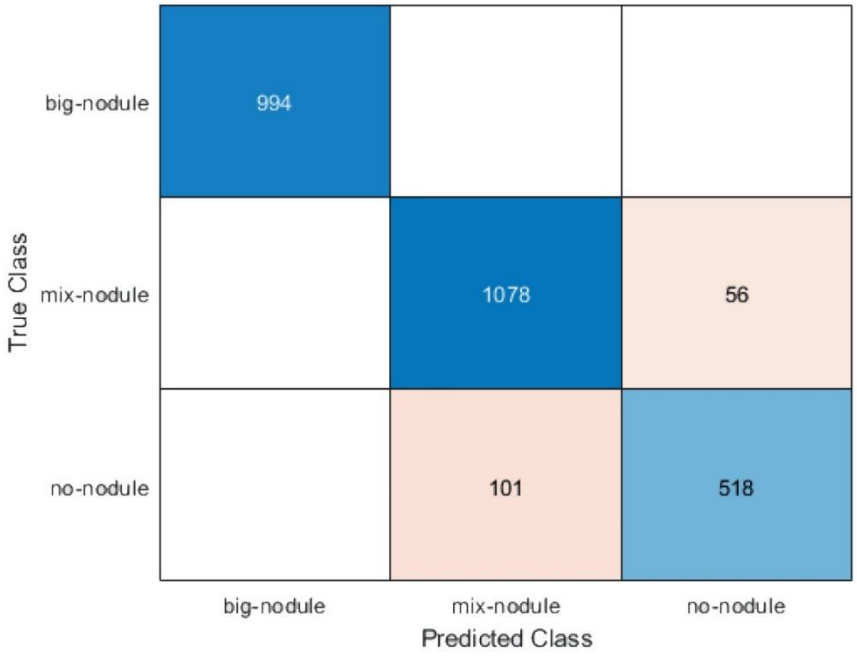

Figure 23 - Result of GLTP

5.2.4. Improved Weber Binary Code (IWBC)

IWBC is more polished form of IWBD and IWLD, combining both since they represent local patterns more efficiently and accurately by using weber magnitude and orientation components [43]. After testing this algorithm on 10% of our entire dataset (the small section that we used to test the accuracy of algorithms) we got 94.43 % accuracy.

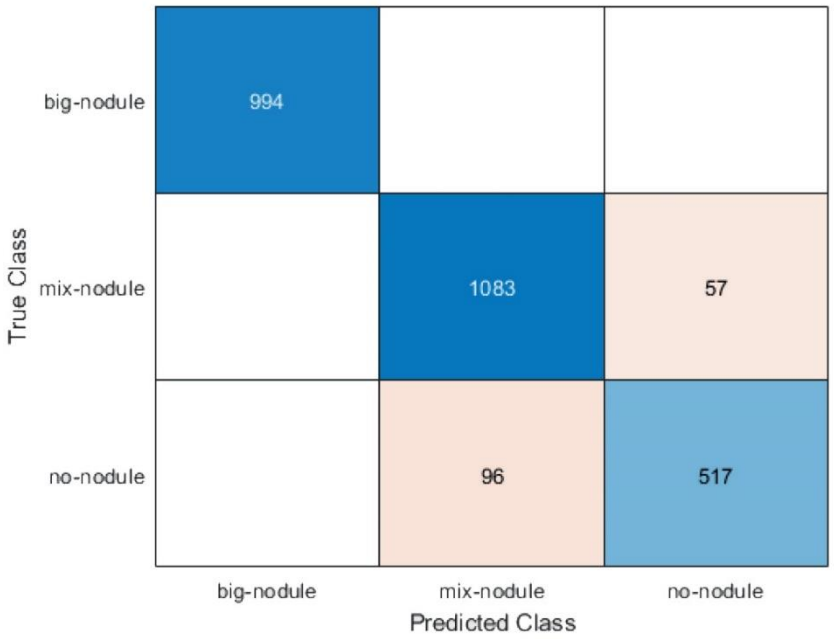

Figure 24 - Result of IWBC

5.2.5. Local Arc Pattern (LAP)

Local arc pattern is a feature based on grey color intensity values, dividing each image into equal sized blocks and histograms of LAP codes then quantizing them to build a classification feature [44]. After testing this algorithm on 10% of our entire dataset (the small section that we used to test the accuracy of algorithms) we got 94.36 % accuracy.

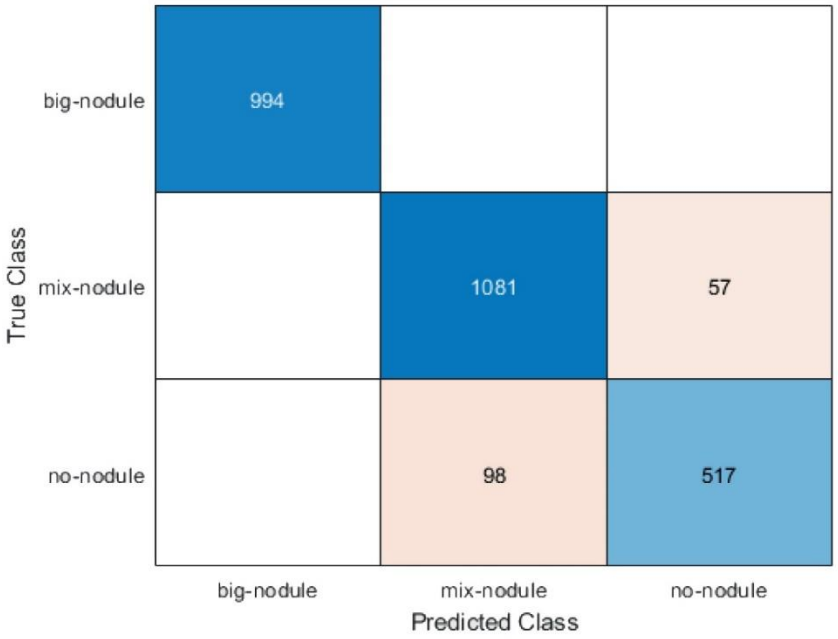

Figure 25 - Result of LAP

5.2.6. Local Binary Patterns (LBP)

Local Binary Pattern (LBP) is a simple and very efficient texture operator that labels image pixels by thresh holding each pixel's neighborhood and considers the result as a binary number. The approach is based on understanding that certain local binary patterns, called "uniform," are fundamental properties of local image texture, and a very strong texture function is proven to be their frequency histogram. It derives a generalized gray-scale and rotation invariant operator presentation that enables the identification of uniform patterns for any angular space quantization and any spatial resolution and provides a mechanism for combining several operators for multi- resolution analysis [45]. After testing this algorithm on 10% of our entire dataset (the small section that we used to test the accuracy of algorithms) we got 93.88 % accuracy.

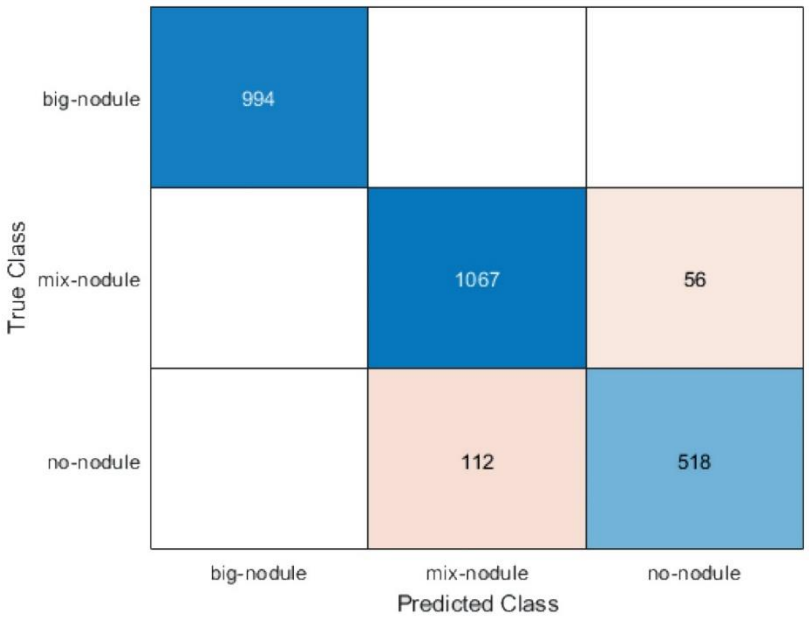

Figure 26 - Result of LBP

5.2.7. Local Directional Pattern (LDiP)

Local Directional pattern is a local feature descriptor, this descriptor computes the edge response at each pixel position in all eight directions and generating a code from relative magnitude strength. This is robust in noisy situation because every code sequence is determined considering local neighborhood. It also has a rotation invariant LDP code which uses the direction of the most prominent edge response [46]. After testing this algorithm on 10% of our entire dataset (the small section that we used to test the accuracy of algorithms) we got 93.85 % accuracy.

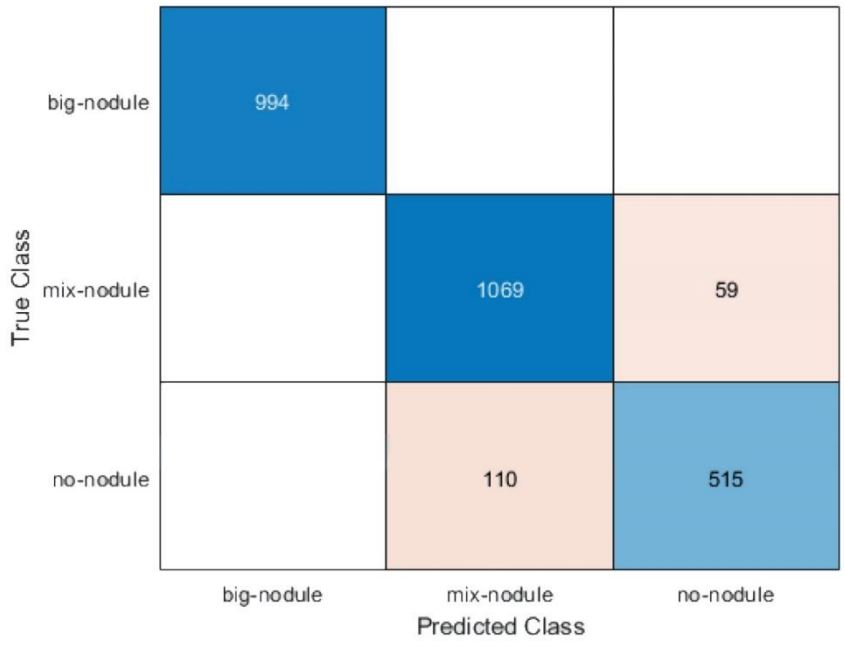

Figure 27 - Result of LDiP

5.2.8. Local Direction Pattern Variance (LDiPV)

LDiPV is a more polished descriptor as compared to LDP, LDiPV introduces a local variance of directional response in order to encode the contrast data within the same descriptor [47]. After testing this algorithm on 10% of our entire dataset (the small section that we used to test the accuracy of algorithms) we got 93.88 % accuracy.

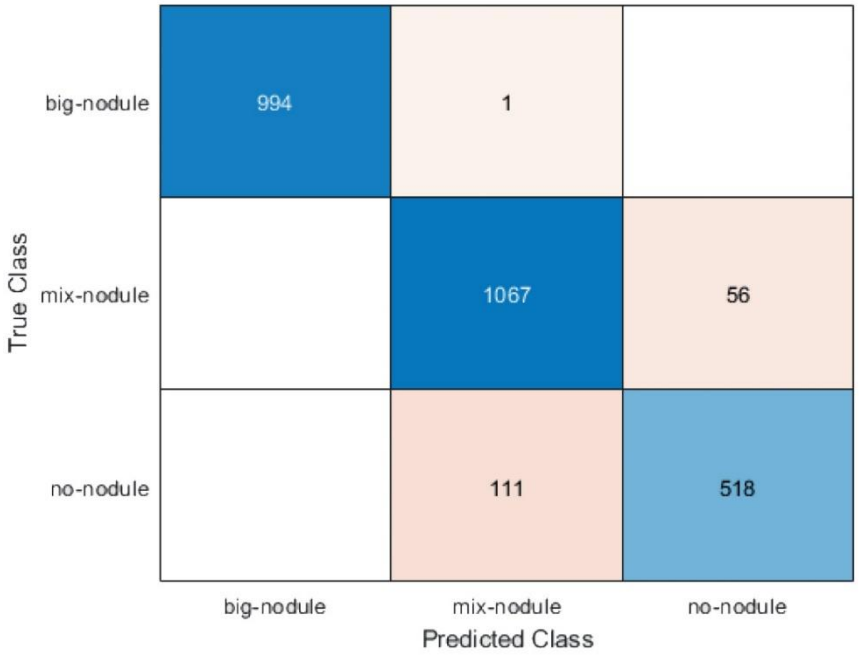

Figure 28 - Result of LDiPV

5.2.9. Local Directional Number Pattern (LDN)

Local Directional Pattern is a descriptor which encodes the directional data in a compact way producing more distinctive code as compared to other methods. It computes structure of each micro pattern using compass mask, which extracts directional info, after that in order to distinguish among similar structural pattern with different intensity transition this information is encoded in prominent direction indexes and sign [48]. After testing this algorithm on 10% of our entire dataset (the small section that we used to test the accuracy of algorithms) we got 94.61 % accuracy.

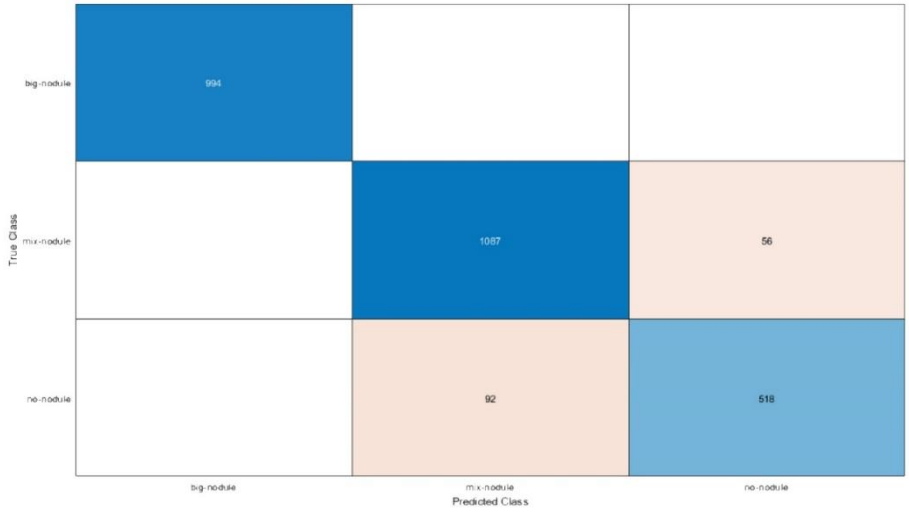

Figure 29 - Result of LDN

5.2.10. Local Gabor Binary Pattern Histogram Sequence (LGBPHS)

Local Gabor Binary Pattern Histogram Sequence is a descriptor which uses histograms as suggested by name, it converts images into histogram sequence by concatenating the histograms of all gabor magnitudes binary maps, then histogram intersection is used for recognition and measure similarity and nearest neighborhood is exploited for final result [49]. After testing this algorithm on 10% of our entire dataset (the small section that we used to test the accuracy of algorithms) we got 94.39 % accuracy.

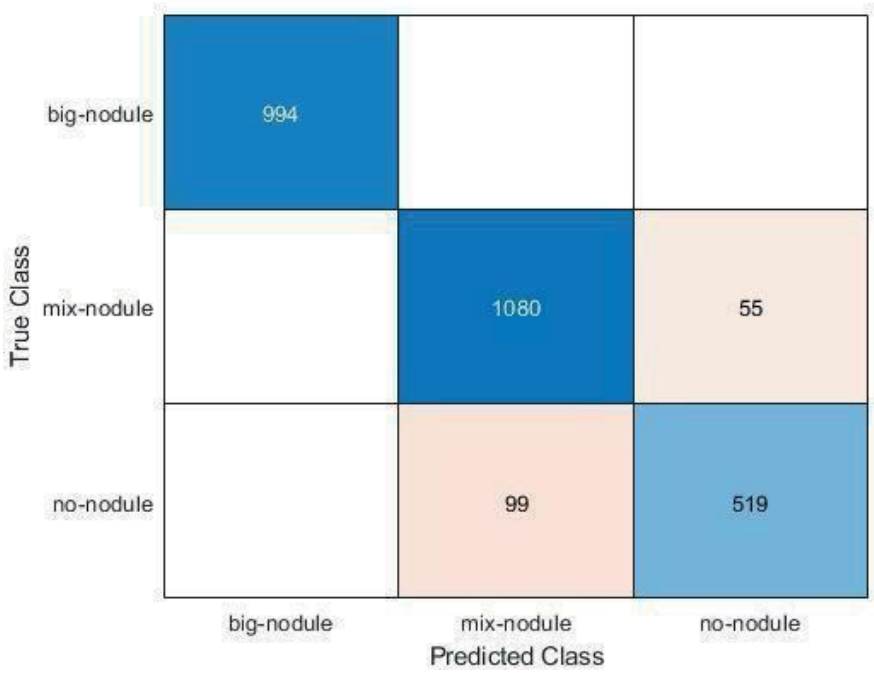

Figure 30 - Result of LGBPHS

5.2.11. Local Gradient Increasing Patter (LGIP)

The Local Gradient Increasing Pattern (LGIP) operator combines the gradient strengths, uniform patterns, and LDP. It describes the increasing trend in local intensity and has good stability to changes in noise and non-monotonic illumination. Using eight binary bits, an LGIP function encodes the intensity-growing patterns in eight directions at each pixel and then assigns a decimal code to define the overall increasing trend. The LGIP histogram relies on a facial descriptor that contains information on the pixel, regional, and global levels. Thus, the descriptor demonstrates supporting discriminativeness for expression of the description [50]. After testing this algorithm on 10% of our entire dataset (the small section that we used to test the accuracy of algorithms) we got 98.87 % accuracy.

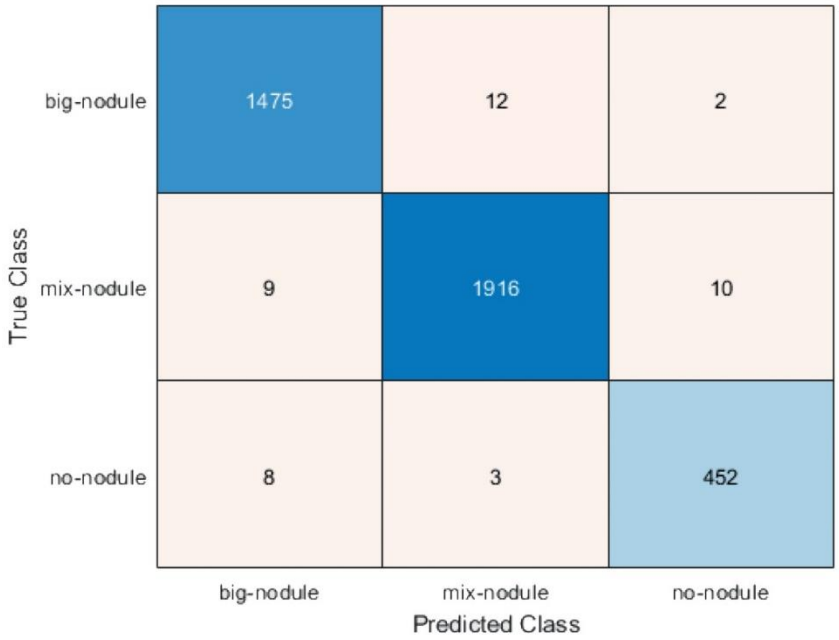

Figure 31 - Result of LGIP

5.2.12. Local Gradient Pattern (LGP)

Local Gradient Pattern is a simple facial pattern descriptor for facial expression recognition. The local pattern is determined based on the spatial gradient flow across the central pixel in a separate pixel area from one side to another. Two independent two-bit binary patterns reflect the central pixel of the area, named for the pixel as Local Gradient Patch (LGP). LGP descriptor is extracted from each pixel. The facial image is divided into 81 blocks of equivalent size, and the histograms of local LGP features are concatenated to create the feature vector for all 81 blocks [51]. After testing this algorithm on 10% of our entire dataset (the small section that we used to test the accuracy of algorithms) we got 94.36 % accuracy.

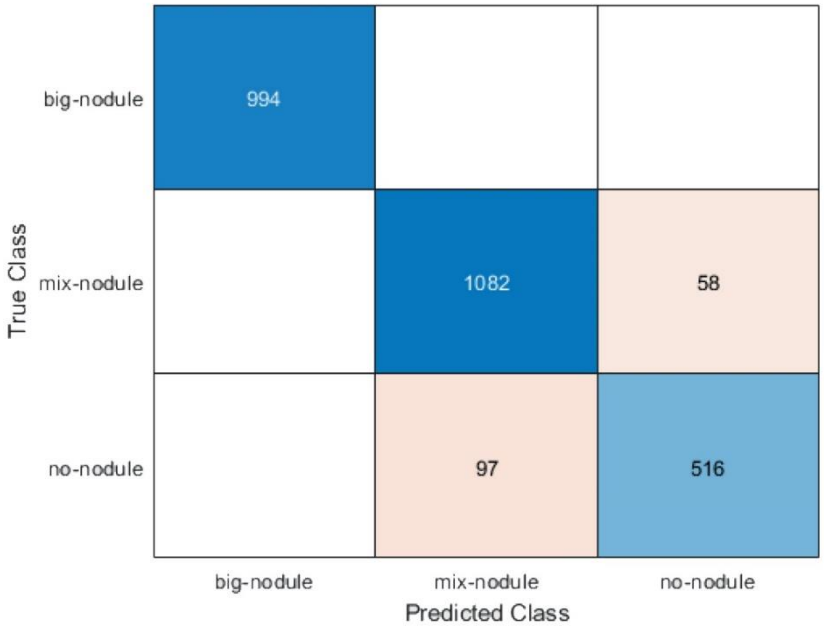

Figure 32 - Result of LGP

5.2.13. Local Monotonic Pattern (LMP)

Local Monotonic Pattern (LMP) can extract strong facial features from a face image that provides accurate and reliable expression recognition efficiency. The LMP operator applied to a pixel finds the monotonic intensity change of the neighboring pixel at different radii. The micropatterns therefore find enhancement by carving the images of each tile and taking histograms with spatial information. The resulting vector is a histogram snapshot [52]. After testing this algorithm on 10 percent of our whole dataset (the small portion we used to check algorithm accuracy), we obtained 93.85 % accuracy.

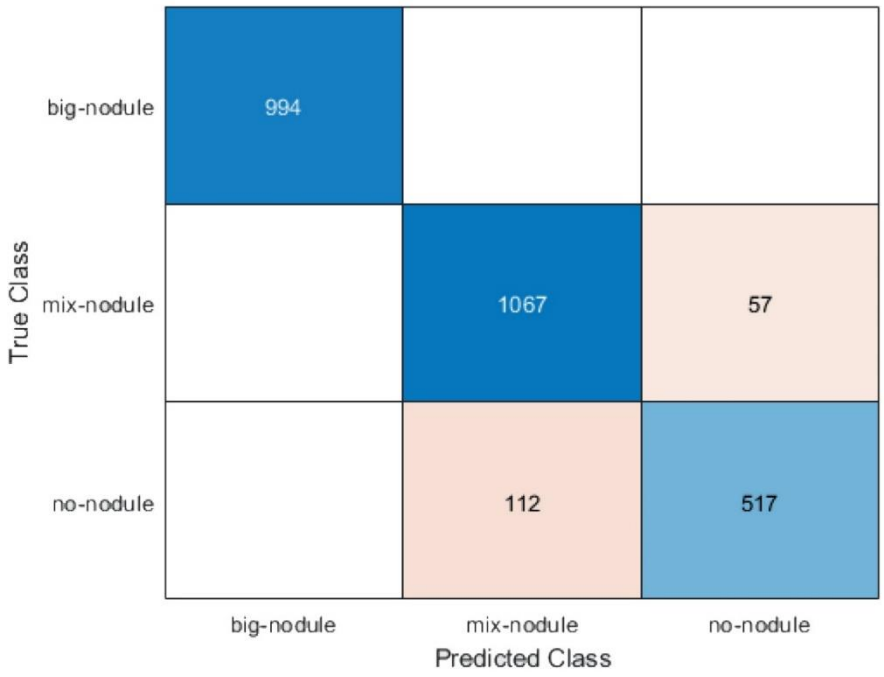

Figure 33 - Result of LMP

5.2.14. Monogenic Binary Coding (MBC)

Monogenic Binary Coding is an efficient local feature extraction scheme for the representation and identification of face. The representation of the monogenic signal decomposes an original signal into three complementary components: amplitude, orientation, and phase. Encode the monogenic variance in each local area and the monogenic feature in each pixel, then measure the statistical characteristics (e.g., histogram) of the local features extracted. The local statistical feature derived from the monogenic complementary components (i.e., amplitude, direction, and phase) is then fused for successful FR. One of the key benefits of the MBC descriptor is its low time and space complexity, thus maintaining very good efficiency with the LSF-FR methods based on the Gabor feature [53]. After testing this algorithm on 10% of our entire dataset (the small section that we used to test the accuracy of algorithms) we got 94.07 % accuracy.

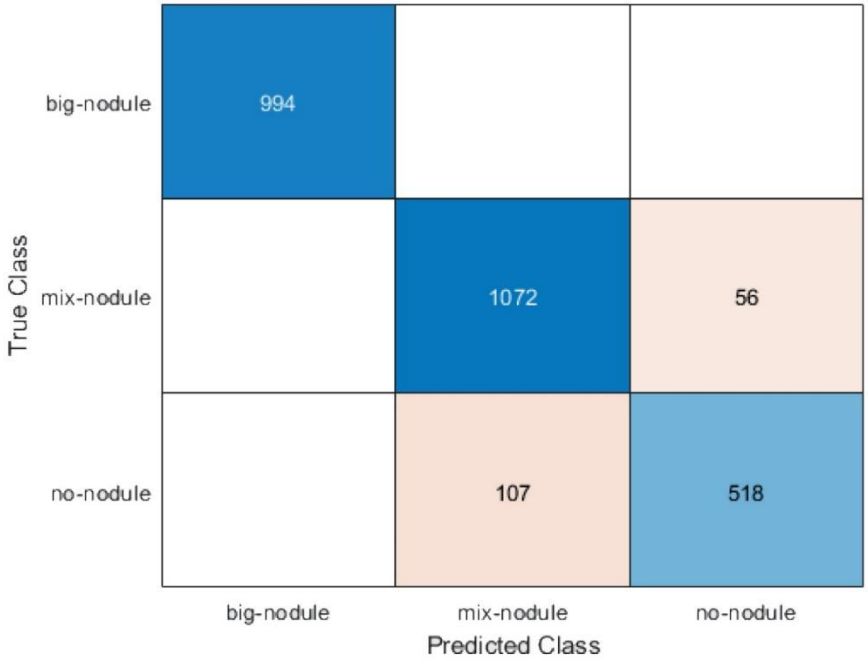

Figure 34 - Result of MBC

5.2.14 Median Robust Extended Local Binary Pattern (MRELBP)

MRELBP is an extended and polished form of LBP, specifically to address image noise problem. This descriptor compares regional image medians instead of raw image intensities. Because this addition MRELBP is good for both micro and macro structure texture info [54]. After testing this algorithm on 10% of our entire dataset (the small section that we used to test the accuracy of algorithms) we got 94.43 % accuracy.

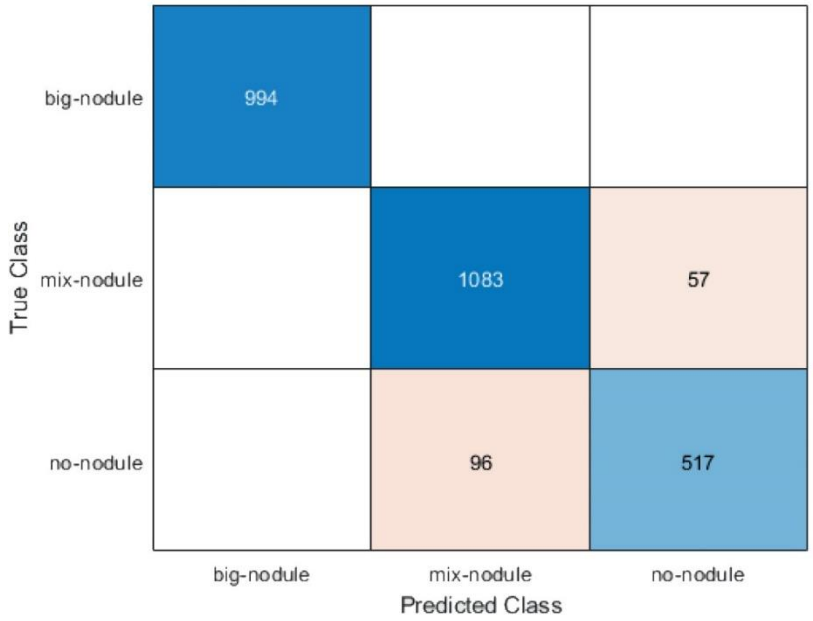

Figure 35 - Result of MRELBP

5.2.15. Median Ternary Pattern (MTP)

Median Ternary Pattern is a descriptor where the operator encodes texture data of local neighborhood by thresholding against local grey scale value and quantizing intensity value of neighbors around each pixel into 3 levels [55]. After testing this algorithm on 10% of our entire dataset (the small section that we used to test the accuracy of algorithms) we got 93.78 % accuracy.

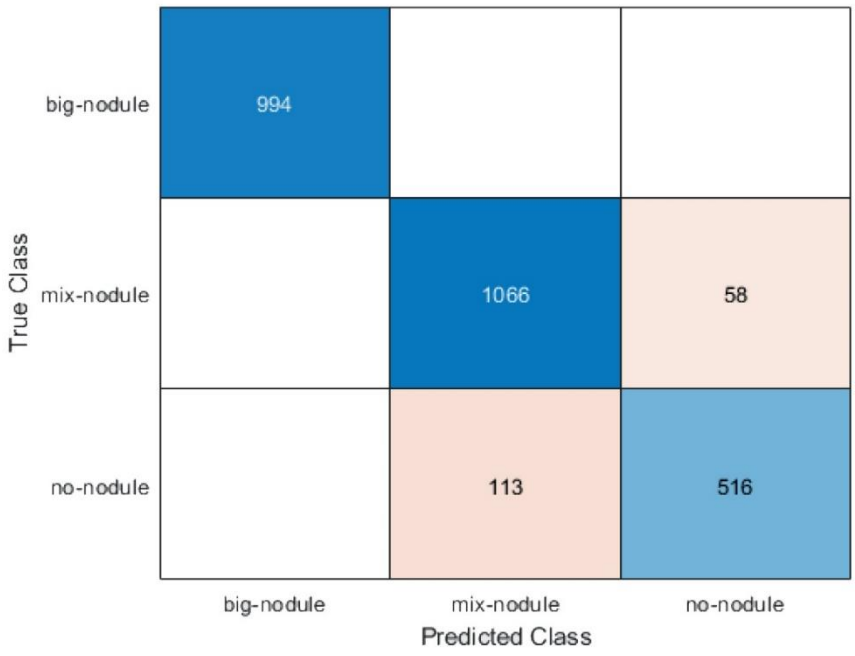

Figure 36 - Result of MTP

5.2.16. Weber Local Descriptor (WLD)

Weber local descriptor is a descriptor inspired by Weber's law, the main component for this descriptor is the gradient of images, this descriptor work with the gradient of images for computing image texture [56]. After testing this algorithm on 10% of our entire dataset (the small section that we used to test the accuracy of algorithms) we got 94.54 % accuracy.

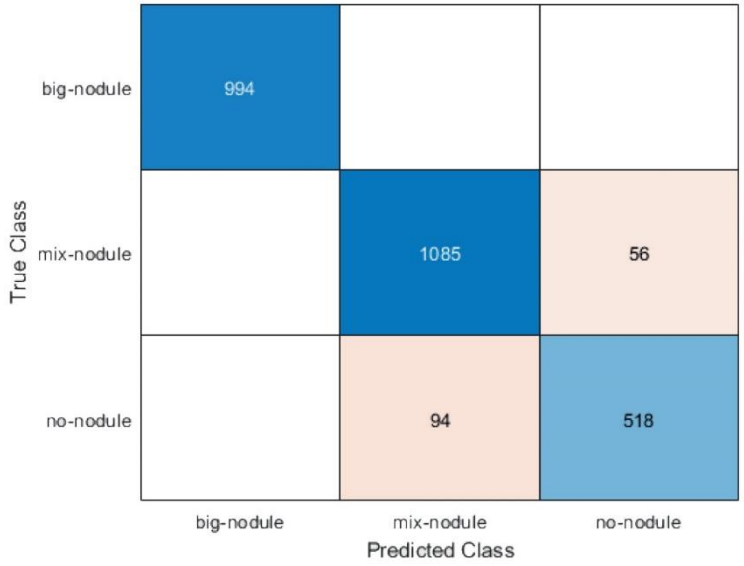

Figure 37 - Result of WLD

5.2.17. Histogram of Oriented Gradients (HOG)

Histogram of oriented gradients is a feature descriptor which operated on the gradient of images both vertical and horizontal and make histogram in order to compute and process images. The HOG descriptor of an image patch is usually visualized by plotting the 9×1 normalized histograms in the 8×8 cells [57]. After testing this algorithm on 10% of our entire dataset (the small section that we used to test the accuracy of algorithms) we got 93.59 % accuracy.

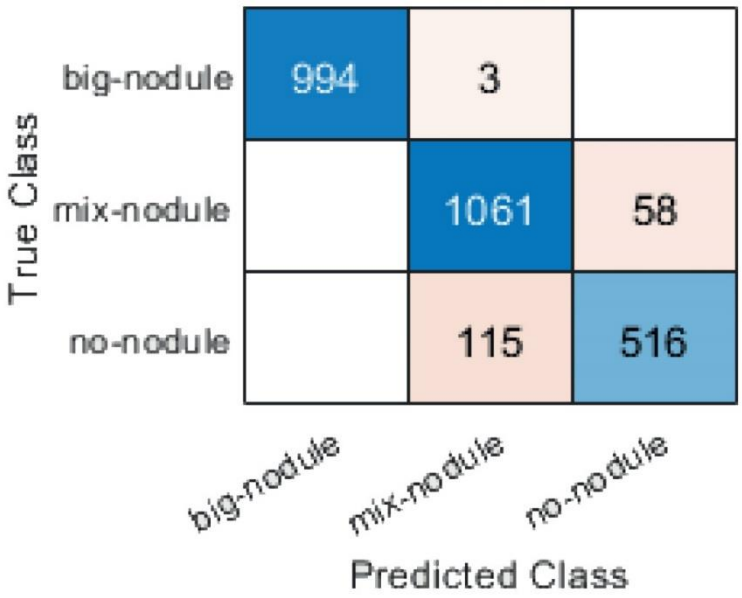

Figure 38 - Result of HOG

Here is the summary table of all hand crafted descriptor experiments:

Table 5 – summary of hand crafted descriptor test results

DESCRIPTOR	ACCURACY
BPPC	93.57%
GDP	94.28%
GLTP	94.28%
IWBC	94.43%
LAP	94.36%
LBP	93.88%
LDiP	93.85%
LDiPV	93.88%
LDN	94.61%
LGBPHS	94.39%
LGIP	98.87%
LGP	94.36%
LMP	93.85%
MBC	94.07%
MRELBP	94.43%
MTP	93.78%
WLD	94.54%
HOG	93.59%

All the test results of both categories are combine in following chart:

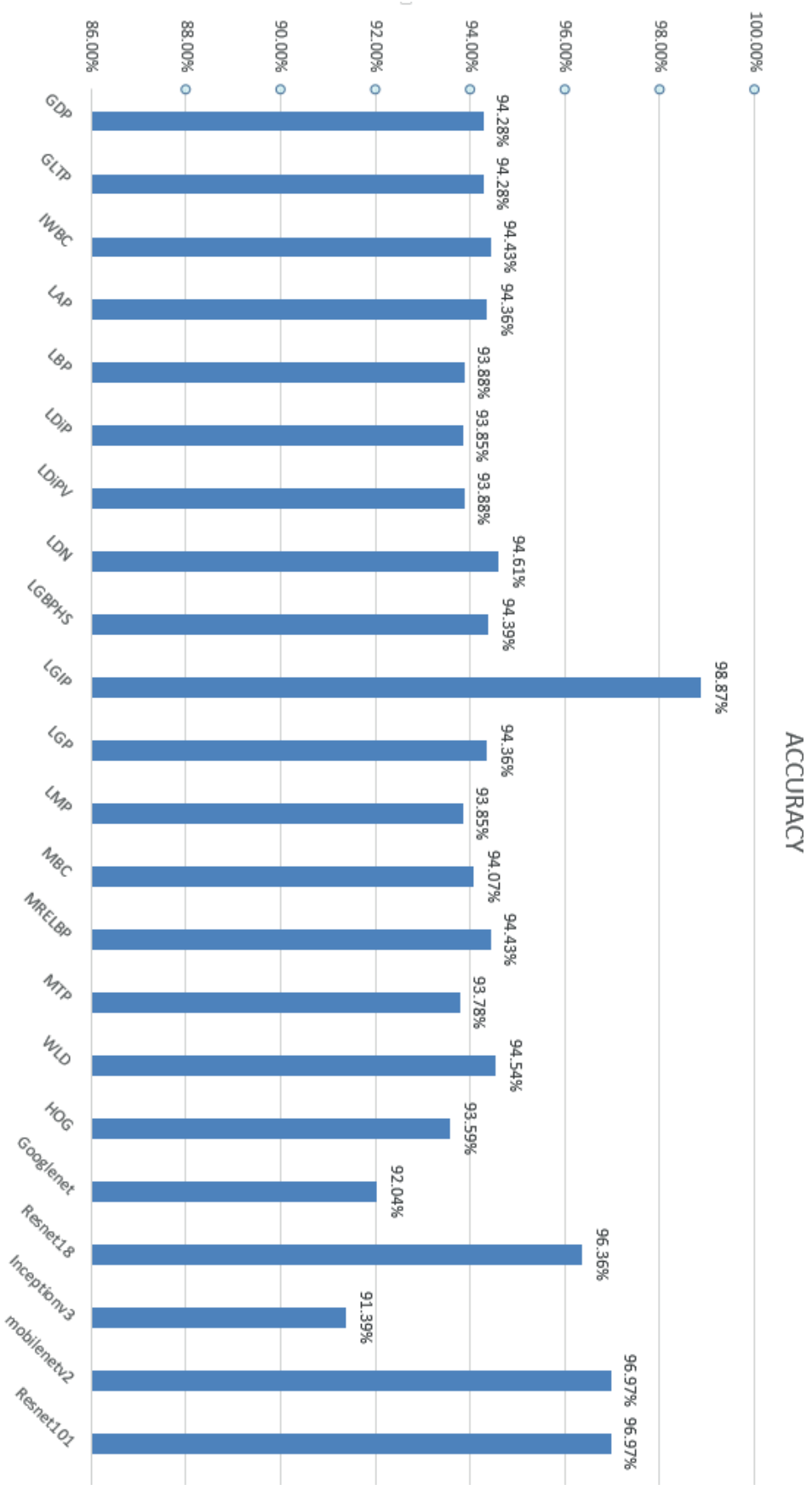

CHAPTER VI

6.1 Proposed Descriptor

6.1.1 LGiP (Local Gradient Increasing Pattern)

LBP feature allots every pixel with 8 parallel pieces by comparing the power with its 8 neighbors, and afterward changes over them to a decimal mark, as communicated in.

$$LBP(x_c, y_c) = \sum_{p=0}^{7} s(i_p - i_c)2^p,\ s(x) = \begin{cases} 1, x \geq 0 \\ 0, x < 0 \end{cases} \quad (1)$$

Where i_p is the force of p^{th} neighbor and i_c is power of focal pixel. Generally, there are 2^8

= 256 examples. One most as often as possible utilized LBP variation is to utilize uniform examples to re-duce the dimensionality to 59. LDP highlight convolves the nearby power fix with eight Kirsch edge covers, and sets initial three bearings with most noteworthy reactions as 1, and others as 0. Absolutely, there are ${}^8C_3$ = 56 examples. One downside is the expanding computational expense from ascertaining and ranking the eight Kirsch edge reactions.

The proposed LGIP is intended to communicate the bearing and extent of nearby power expanding pattern. Initial, eight Sobel covers M0, M1, M7 as appeared in fig. 1 are utilized to figure angle reactions in eight directions at every pixel. At that point the pixel is appointed with a 8- piece code as per the indications of the eight reactions. We set those bearings with positive reactions as 1 and others as 0. For instance, the force pattern in fig. 3(a) can be encoded by 0011 1010 as appeared in fig. 2(a). 1-esteemed piece implies the power expanding pattern is askew as the bolt demonstrates in fig. 1, while 0 methods the pattern is inverse to the bolt. On the other hand, the eight pieces can be chosen by power correlations between focal pixel and its neighbors to accelerate figuring, as LBP administrator. In this work, we receive Sobel slope operator to expand the dependability within the sight of non-uniform enlightenment changes and irregular clamor. Still it is quicker than Kirsh edge administrator in LDP as less pixels and augmentations are included.

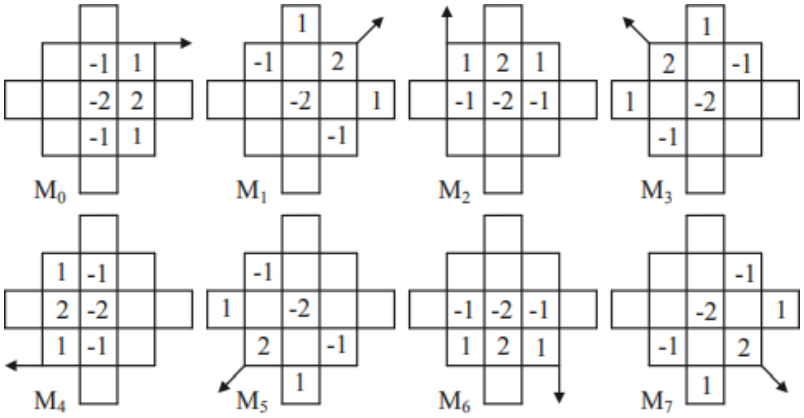

Figure 39 - LGIP feature descriptor explanation

Power expanding patterns in every direction are from focal pixel to 1-esteemed neighbors or from 0-esteemed neighbors to focal pixel. As appeared in fig. 2(a), these patterns are depicted as vectors with unit L∞-standard length, named pattern vectors (TVs). By and large pattern vector (OTV) is characterized as the total of the eight pattern vectors, which comprise of 1-esteemed (dim) and 0-esteemed (dark) vectors. Note the total of 1-esteemed vectors equivalents to the total of 0-esteemed vectors. In this way, the OTV can equally determine as the whole of just 1-esteemed vector. Total of 1-esteemed pattern vectors at that point can similarly computed as the slope of the eight twofold pieces as appeared in the figure. At long last, a LGIP code is doled out to the OTV utilizing a 2D look-into table in fig. 2(b). For example, the OTV of 0011 0101 example in fig. 2 is −2, 1, and the LGIP design is 17. Absolutely, 37 LGIP designs are incorporated.

LGIP has numerous great properties that cause it to beat LBP and LDP. To begin with, LGIP acquires the qualities of great LBP: basic, quick and invariant to monotonic in-strained quality changes. Second, LGIP exploits slope and uniform examples. For a certain something, bigger LGIP code in fig. 2(b) infers the neighborhood force has more one-sided inclination a particular way (OTV course). For something else, huge LGIP designs are a long way from focus in the table. They generally have a place with uniform examples, and speak to the most informative miniaturized scale structures like edges and corners. For instance, LGIP design 35 compares to 8-piece code 0000 0111, 1000 1111, and example 31 relates to 0011 1100. Third, LGIP has great solidness within the sight of repetitive sound non-monotonic power changes like LDP.

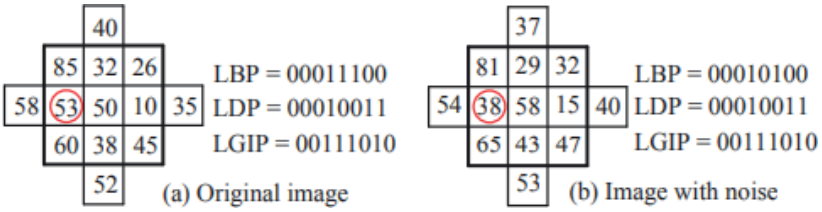

Figure 40 - LGIP feature descriptor explanation

For example, fig. 41 shows the original picture and corresponding picture in the wake of including repetitive sound (pixel). In-strained quality raises in the southeast and drops in the northwest. Fifth piece of LBP changes from 1 to 0 in view of the repetitive sound. Since slope administrator is sufficiently steady, LGIP code holds the equivalent in nearness of such including clamor. At long last, dimensionality of LGIP is lower than both LBP and LDP It can accelerate picture to-picture separation computation [50].

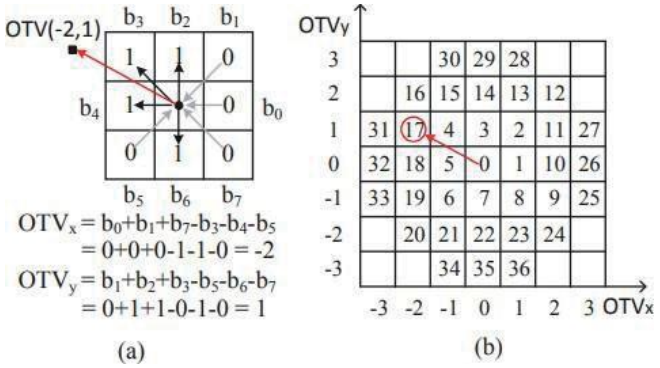

Figure 41 - LGIP feature descriptor explanation

6.1.2 Finalizing results by LGiP

Since LGiP was a great success in testing phase, bringing awesome accuracy of 98.8% to the table, we were sure we found our winner among all the feature descriptors and architectures. We then further the same LGiP descriptor on our entire dataset a few times (each time changing the cell size (between 1 2 4 5 8 10), following are the 3 example results obtained during this period.

Cell Size 2

```
# of Incorrect Recognized Samples=751  and Accuracy=98.08
```

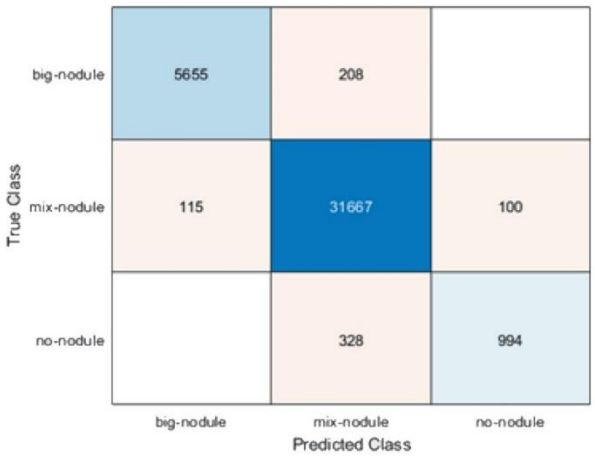

Figure 42 - Result of LGIP on full dataset at cell size = 2

Cell Size 4

```
# of Incorrect Recognized Samples=712  and Accuracy=98.18
```

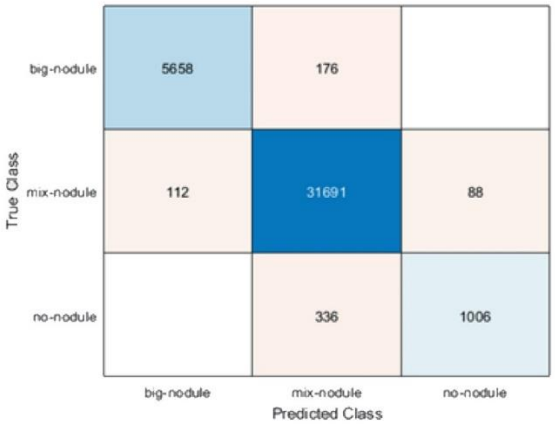

Figure 43 - Result of LGIP on full dataset at cell size = 4

Cell Size 5

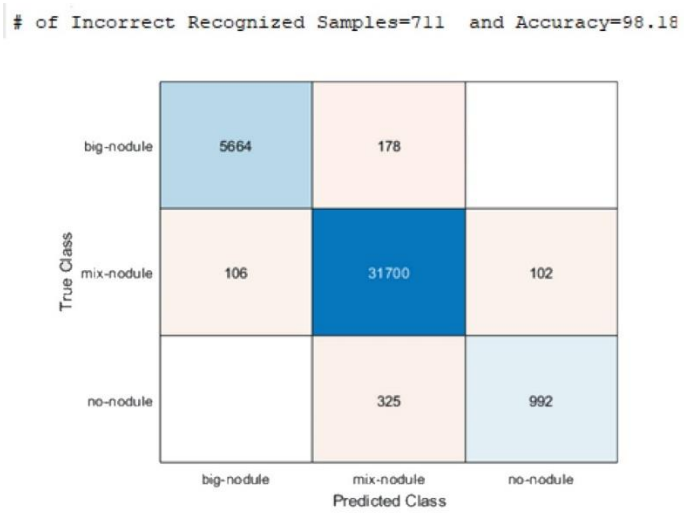

Figure 44 - Result of LGIP on full dataset at cell size = 5

As you can see above, the best possible accuracy achieved was 98.18%, at cell size 4 & 5, although both cell sizes achieved exactly same accuracy, but in convolutional matrix some difference can be seen.

CHAPTER VII

7.1 Results

7.1.1 Future Work

As mentioned multiple times in this report every 0.1% accuracy of cancer diagnosis related to human lives, therefore 98.18% is still not best, increasing the accuracy as high as possible in future with better algorithms would be more beneficial.

How can it be done?

- Combine multiple architectures together.
- Come up with better architectures.
- Better technology to take machine learning to next level.
- Add image segmentation, since here we used whole images.

And last but not least, one day seeing these machine learning approaches implemented in hospitals around the world (but of course not until they have been perfected).

7.1.2 Conclusion

We started with downloading the LIDC database which is publically available for research purposes for anyone who is willing to work on any sort of research regarding Lung Cancer, the details of dataset are mentioned in Chapter Three Section 3.3, afterwards since the dataset had images in '.dcm' format, we used MICRODICOM software to convert the entire dataset into JPEG images in order to feed them to our algorithms for image processing, after that with help of XML files and patient data table excel file (both included in dataset) we divided the entire dataset into 3 sub categories, Benign (just big nodules), malignant (mix nodules of both larger than 3mm and smaller) and Non-cancerous (no-nodules). Since after this the dataset was still too large containing close to 200,000 images of 1000+ patients, we took a small part of the dataset (10% of entire dataset) for our testing phase. Before entering the testing phase we started working on the literature review, and went through about 30 different papers who worked on lung cancer diagnosis through machine learning and extracted the accuracy from those paper in order to learn what is the maximum achieved accuracy that we have to beat in this project,

all details are in Chapter Two and the accuracies in Table 1. Then we started by testing numerous deep learning architectures on

our 10% test dataset, but were able to achieve a maximum of 96.97% (resnet101 & mobilnetv2)

and that was not enough since from past work on this topic the maximum achieved accuracy was 97% ('Pulmonary Tumor Management Volume Detection from Positron Emission Tomography Images' and 'Preventive Health Care Image and Diagnosis Techniques'); So then we started diving into hand crafted descriptors, we tested around 20 different hand crafted descriptors (Chapter Five) on our test dataset and were able to achieve accuracy as high as 98.8% - 98.9% (from LGIP), Then we further ran the same LGIP descriptor on entire 100% of our dataset with different cell sizes (1 2 4 5 8 10) and finally concluded to obtain the best possible accuracy at 98.18% by LGIP at cell size = 4 & 5. This is the highest accuracy by far using any architecture or descriptor.

REFERENCES

[1] World health organization Cancer: ww.who.int/gho/ncd/mortality_morbidity/cancer/en

[2] American Cancer Society: Cancer Facts and Figures. Atlanta: American Cancer Society (2006).

[3] https://zana.com/a/lung-cancer-introduction.2995 Mon, 24 Feb 2020-14:46:48 UTC.

[4] Xing CHEN, Mingfu CAO, Yan Hao Proceedings of the 2005 IEEE Engineering in medical and Biology 27th Annual Conf. China Sep 1-4, 2005.

[5] Noha Lee, Andrew F. LAine, Guillermo, Jeffrey and John K. Gohagan IEEE Review in Bio Medical Engineering, vol 2, 2009.

[6] David S paik, Christipher, Geoffrey, rubeen, Rubak Acar, Joyoni Dey and Sandy Nepel: IEEE Transactions on Medical Iamaging vol 23 No 26, June 2004.

[7] Jyh-Shyan, Shih-Chung, Akira, Mattew and Seong: IEEE Transactions on Medical Iamaging vol 15, No 2, April 1996.

[8] M. Freedman, "Improved small volume lung cancer detection with computer-aided detection: Database characteristics and imaging of response to breast cancer risk reduction strategies," Ann. NYAcad. Sci., vol. 1020, pp. 175–89, 2004.

[9] R. MacRedmond., "Screening for lung cancer using low dose CT scanning," Thorax, vol. 59, pp. 237–41, 2004

[10] Basavanna, "Tumor Cell Identification in Medical Images using Image Processing Tech- niques" October, 2016.

[11] Z. Liu and M. Tan, "ROC-based utility function maximization for feature selection and classification with applications to high-

dimensional protease data, biometrics," J. Int. Bio- metr. Soc., vol. 64, no. 4, pp. 1155–1161, 2008.

[12] Bhagyasri G. Patil, Prof Sanjeev "Cancer cells Detection using Digital Image Processing Methods", Vol 3 Issue 4 March 2014.

[13] Dansheng Song, Tatyana A. Zhukov, Olga Markov, Wei Qian, Melvyn S. Tockman, "Prog- nosis of stage i lung cancer patients through quantitative analysis of centrosomal features", ie, pp: 1607-1610, 3012.

[14] Fatma Taher, Naoufel Werghi and Hussain Al-Ahmed, "Bayesian Classification Artificial Neural Network Methods for Lung Cancer Early Diagnosis", IEEE, pp: 773-776, 2012.

[15] Prasshanth Naresh, Rajashree Shettar, "Image Processing and classification Techniques for early Detection of Lung Cancer for Preventive Healthcare: October, 2016.

[16] Aparna Kanakatte, Nallasamy Mani, Bala Srinivasan, Jayavardhana Gubbi, "Pulmonary Tumor Volume Detection from Positron Emission Tomography Images", International Conference on Biomedical Engineering and Informatics, pp: 213-217, 2008.

[17] Yongbum Lee, Takeshi Hara, Hiroshi, shigeki and Takeo: IEEE Transactions on Medical Iamaging vol 20 No 7, July 2001.

[18] Samuel H Hawkins, Yoganand Balagurunathan, Virendra kumar, Lawrence, and Robert IEEE Access, vol 2, 2014.

[19] Anam Tariq, M. Usman Akram and M. Younus Javed, "Lung Nodule Detection in CT Ima- ges using Neuro Fuzzy Classifier", Fourth International Workshop on Computational Intel- ligence in Medical Imaging (CIMI), pp: 49-53, 2013.

[20] Ruchika, Ashima "Detection of Lung cancer in CT Images using Mean Shift Algorithm", volume 5, issue 5, May 2015.

[21] J. Gohagan., “Baseline findings of a randomized feasibility trial of lung cancer screening with spiral CT scan vs chest radiograph: The lung screening study of the National Cancer Institute,” Chest, vol. 126, pp. 114–21, 2004.

[22] Kesav Kancherla, Srinivas Mukkamala, “Early Lung Cancer Detection using Nucleus Seg- mentation based Features”, IEEE Symposium on Computational Intelligence in Bioinfor- matics and Computational Biology (CIBCB), pp: 91-95, 2013.

[23] R. Sah., “Results of surgical treatment of stage I and II lung cancer,” J. Cardiovasc. Surg., vol. 37, pp. 169–172, 1996.

[24] S. Sone., “Mass screening for lung cancer with mobile spiral computed tomography scan- ner,” Lancet, vol. 351, pp. 1242–5, 1998.

[25] B. S. Kramer and O. W. Brawley, “Cancer screening,” Hematol. Oncol. Clin. North Amer., vol. 14, pp. 831–48, 2000.

[26] J. C. Nesbitt., “Survival in early-stage lung cancer,” Ann. Thorac. Surg., vol. 60, pp. 466– 472, 1995.

[27] B. J. Flehinger, M. Kimmel, and M. R. Melamed, “Survival from early lung cancer: Impli- cations for screening,” Chest, vol. 101, pp. 1013–1018, 1992

[28] M. Aoyama, Q. Li, S. Katsuragawa, H. MacMahon, and K. Doi, “Automated computerized scheme for distinction between benign and malignant solitary pulmonary nodules on chest images,” Med. Phys., vol. 29, pp. 701–8, 2002.

[29] L. L. Humphrey, S. Teutsch, and M. Johnson, “Lung cancer screening with sputum cyto- logic examination, chest radiography, and computed tomography: An update for the U.S. Preventive Services Task Force,” Ann. Intern. Med., vol. 140, pp. 740–

53,2004.

[30] C. I. Henschke., “CT screening for lung cancer: Suspiciousness of nodules according to size on baseline scans,” Radiology, vol. 231, pp. 164–8, 2004.

[31] https://medium.com/ml-research-lab/machine-learning-algorithm-overview-5816a2e6303 Thu, 26 Mar 2020- 10:55:14 UTC.

[32] https://victorzhou.com/blog/intro-to-cnns-part-1/ Thu, 26 Mar 2020- 22:30:50 UTC.

[33] https://www.ncbi.nlm.nih.gov/pmc/articles/PMC3041807 Fri, 17 Jan 2020- 13:23:54 UTC.

[34] https://wiki.cancerimagingarchive.net/display/Public/LIDC-IDRI Sun, 29 Dec 2019- 19:58:23 UTC.

[35] https://machinelearningmastery.com/transfer-learning-for-deep-learning/ Fri, 05 June 2020- 02:37:44 UTC.

[36] https://www.mathworks.com/help/deeplearning/ref/resnet18.html?s_tid=srchtitle Wed, 29 July 2020- 20:17:20 UTC.

[37] https://www.mathworks.com/help/deeplearning/ref/inceptionv3.html?s_tid=srchtitle Sat, 30 May 2020- 18:43:04 UTC.

[38] https://www.mathworks.com/help/deeplearning/ref/mobilenetv2.html?s_tid=srchtitle Sun, 05 July 2020- 08:45:44.

[39] https://www.mathworks.com/help/deeplearning/ref/resnet101.html?s_tid=srchtitle Wed, 20 May 2020- 00:44:55 UTC.

[40] Seyedehsamaneh Shojaeilangari, Wei-Yun Yau, Jun Li, Eam-Khwang Teoh “Feature Extraction through Binary Pattern of Phase Congruency for Facial Expression Recognition” 12th International Conference on Control, Automation, Robotics & Vision Guangzhou,

China, 5-7th December 2012

[41] F. Ahmed “Gradient directional pattern: a robust feature descriptor for facial expression recognition” ELECTRONICS LETTERS 13th September 2012 Vol. 48 No. 19

[42] Faisal Ahmed, Emam Hossain “Automated Facial Expression Recognition Using Gradient- Based Ternary Texture Patterns” Hindawi Publishing Corporation Chinese Journal of Engineering Volume 2013, Article ID 831747

[43] Bao-Qing Yang, Tao Zhang, Chao-Chen Gu, Kai-Jie Wu, Xin-Ping Guan “A novel face recognition method based on IWLD and IWBC” Multimed Tools Appl (2016) 75:6979–7002

[44] Moh. Shahidil Islam, Surapong Auwatanamongkol “Facial Expression Recognition using Local Arc Pattern” Trends in Applied Sciences Research 9(2): 113-120, 2014

[45] Timo Ojala, Matti PietikaÈinen, Topi MaÈenpaÈa “Multiresolution Gray-Scale and Rotation Invariant Texture Classification with Local Binary Patterns” IEEE TRANSACTIONS ON PATTERN ANALYSIS AND MACHINE INTELLIGENCE, VOL. 24, NO. 7, JULY 2002

[46] Taskeed Jabid, Md. Hasanul Kabir, Oksam Chae “Local Directional Pattern (LDP) – A Robust Image Descriptor for Object Recognition” 2010 Seventh IEEE International Conference on Advanced Video and Signal Based Surveillance

[47] Md. Hasanul Kabir, Taskeed Jabid, Oksam Chae “A Local Directional Pattern Variance (LDPv) based Face Descriptor for Human Facial Expression Recognition” structure (LDP) and contrast (variance of local texture) in2010 Seventh IEEE International Conference on Advanced Video and Signal Based Surveillance

[48] Adin Ramirez Rivera, Jorge Rojas Castillo, Oksam Chae, “Local Directional Number Pattern for Face Analysis: Face and Expression Recognition” 2011 IEEE TRANSACTIONS ON IMAGE PROCESSING

[49] Wenchao Zhang, Shiguang Shan , Wen Gao, Xilin Chen, Hongming Zhang “Local Gabor Binary Pattern Histogram Sequence (LGBPHS): A Novel Non-Statistical Model for Face Representation and Recognition” Proceedings of the Tenth IEEE International Conference on Computer Vision

[50] Zhou Lubing, Wang Han, “LOCAL GRADIENT INCREASING PATTERN FOR FACIAL EXPRESSION RECOGNITION” 978-1-4673-2533-2/12/$26.00 ©2012 IEEE

[51] M. Shahidul Islam “Local gradient pattern - A novel feature representation for facial expression recognition” 23 April 2013; accepted 16 June 2013

[52] Tahseen Mohammad, Md. Liakot Ali “Robust Facial Expression Recognition Based on Local Monotonic Pattern (LMP)” Proceedings of 14th International Conference on Computer and Information Technology (ICCIT 2011) 22·24 December, 2011

[53] Meng Yang, Lei Zhang, Simon Chi-Keung Shiu, David Zhang, “Monogenic Binary Coding: An Efficient Local Feature Extraction Approach to Face Recognition” IEEE TRANSACTIONS ON INFORMATION FORENSICS AND SECURITY, VOL. 7, NO. 6, DECEMBER 2012

[54] Li Liu, Songyang Lao, Paul W. Fieguth, Yulan Guo, Xiaogang Wang, Matti Pietikäinen, “Median Robust Extended Local Binary Pattern for Texture Classification” IEEE TRANSACTIONS ON IMAGE PROCESSING, VOL. 25, NO. 3, MARCH 2016

[55] Farhan Bashar∗, Asif Khan, Faisal Ahmed, Md. Hasanul Kabir “Robust Facial Expression Recognition Based on Median Ternary Pattern (MTP)” 2013 International Conference on Electrical Information and Communication Technology (EICT)

[56] LIU Shuaishi1, ZHANG Yan, LIU Kepin, “Facial Expression Recognition under Partial Occlusion Based on Weber Local Descriptor Histogram and Decision Fusion” Proceedings of the 33rd Chinese

Control Conference July 28-30, 2014,

[57] Satya Mallick, https://www.learnopencv.com/histogram-of-oriented-gradients/ Wed, 22 Apr 2020- 19:33:32 UTC.

[58] C. I. Henschke., "Early lung cancer action project: Overall design and findings from base- line screening," Lancet, vol. 354, pp. 99–105, 1999.

[59]D. S. Gierada, T. K. Pilgrim, M. Ford, R. M. Fagerstrom, T. R. Church, H. Nath, K. Garg, and D. C. Strollo, "Lung cancer: inter observer agreement on interpretation of pulmonary findings at low-dose CT screening," Radiol., vol. 246, no. 1, pp. 265–272, 2008.

[60] L. Berlin, "Liability of performing CT screening for coronary artery disease and lung can- cer," Amer. J. Roentgenol., vol. 179, pp. 837–42, 2002.

[61] S. J. Swensen., "Screening for lung cancer with low-dose spiral computed tomography," Amer. J. Respir. Crit. Care Med., vol. 165, pp. 508–13, 2002.

[62] S. Sivakumar, Dr. C. Chandrasekar, "Lung Nodule Detection Using Fuzzy Clustering and Support Vector Machines", International Journal of Engineering and Technology (IJET), Vol 5 No 1, pp: 179-185, Feb-Mar 2013

[63] https://machinelearningmastery.com/start-here/#algorithms Tue, 4 Aug 2020- 09:55:20 UTC.

[64] S. K. Vijai Anand, "Segmentation coupled Textural Feature Classification for Lung Tumor Prediction", ICCCCT, pp: 518524, 2010.

[65] Atiyeh Hashemi, Abdol Hamid Pilevar, Reza Rafeh, "Mass Detection in Lung CT Images Using Region Growing Segmentation and Decision Making Based on Fuzzy Inference

System and Artificial Neural Network", I. J. Image, Graphics and Signal Processing, 6, pp: 16- 24, 2013.

[66] J. A. Swets, "ROC analysis applied to the evaluation of medical imaging techniques," In- vest. Radiol., vol. 14, pp. 109–21, 1979.

[67] https://www.mathworks.com/matlabcentral/fileexchange/64456 - deep-learning-tool-box- model-for-googlenet-network?s_tid=srchtitle Sun, 7 June 2020- 16:14:59 UTC.

[68] Lea Marie Pehrson, Michael Bachmann Nielsen, Carsten Ammitzbøl Lauridsen "Automatic Pulmonary Nodule Detection Applying Deep Learning or Machine Learning Algorithms to the LIDC-IDRI Database: A Systematic Review" Diagnostics2019,9,29;doi:10.3390/diagnostics9010029